Original Manuscript

Journal of LOW FREQUENCY NOISE, VIBRATION AND ACTIVE CONTROL

Journal of Low Frequency Noise, Vibration and Active Control
2025, Vol. 0(0) 1–25

DOI: 10.1177/14613484251401355
journals.sagepub.com/home/lfn
Sage

Probabilistic modeling of spectator jumping loads for temporary grandstands: Insights from experiments and load simulation

Suhui Yu[1], Jian Yuan[1], Shan Gao[2,3], Zhenhua Huang[4], Feng Fu[5] and Zhe Zhang[6]

Abstract

Jumping loads are the most significant form of crowd-induced dynamic loading on temporary grandstands. This study presents experimental results from subjects jumping at frequencies between 1.0 Hz and 3.0 Hz on force plates, analyzing three key parameters: peak load ratio, jumping period, and contact time. A widely used mathematical model for simulating vertical jumping loads is reviewed and refined based on these experiments. The analysis also includes two-person jump dynamics and associated horizontal loads. Results show that the peak load ratio and contact parameters follow truncated normal distributions and can be used to simulate quasi-periodic jumping loads. A Gaussian-based multi-peak model significantly improves computational efficiency for non-single-peak jumps. The combined jumping load from two individuals is approximately 85% of the linear superposition of individual loads. Horizontal loads were also quantified, with front-to-back forces averaging 45% of body weight and side-to-side forces 10%. These findings support more accurate load simulations for safer grandstand design under dynamic crowd conditions and the models are convenient to be applied in the vibration serviceability assessment of stadium stands.

Keywords

jumping load experiment, characteristic parameters, mathematical model, dynamic vibration, temporary grandstand structure

Introduction

Due to their rapid construction, strong adaptability to site conditions, and notable sustainability, temporary grandstands have become the structure of choice for various large-scale outdoor public entertainment and sports activities. Conventional large-scale temporary grandstands are composed of a spatially hinged steel bar system and have a low natural frequency, making them prone to local or even global vibrations when subjected to low-frequency dynamic loads from spectators. Such vibrations may lead to crowd panic and even structural collapse, as shown in Figure 1, where a grandstand collapsed due to jumping spectators during a football game on 17 October 2021, and the reason of the collapse were analyzed by some researches.[1–3] In fact, numerous accidents have demonstrated that excessive spectator load is an important cause of both permanent and temporary grandstand collapse.[4] Therefore, accurately calculating spectator jumping loads is critical for informing structural design codes and safety guidelines.[5–9] Because different countries vary in culture and physique, and individuals differ in behavior, the peak ratios, jumping periods, and contact times of jumping loads can vary significantly.

[1]Academy of Combat Support, Rocket Force University of Engineering, Xi'an, China
[2]Shaanxi Key Laboratory of Safety and Durability of Concrete Structures, Xijing University, Xi'an, China
[3]Key Lab of Structures Dynamic Behavior and Control of the Ministry of Education, Harbin Institute of Technology, Harbin, China
[4]Departments of Mechanical Engineering and Data Science, University of North Texas, Denton, TX, USA
[5]Department of Engineering, School of Science & Technology, City, University of London, London, UK
[6]College of Civil Engineering, Nantong Institute of Technology, Nantong, China

Corresponding author:
Shan Gao, Key Lab of Structures Dynamic Behavior and Control of the Ministry of Education, Harbin Institute of Technology, Huanghe Road No. 73, Harbin, China.
Email: 13833185232@139.com

These parameters are fundamental to load calculations. Accurately representing the diversity and randomness of jumping loads to reflect actual spectator behavior has become a critical and urgent area of structural safety research. Although several jumping load models exist, there remains a need for reliable theoretical frameworks to support load calculations for large-scale temporary grandstands. Early researchers utilized a simple half-sine function to fit measured jumping forces.[10–12] But the real forces are not to equivalent perfectly periodic simulation.[13] Then, some researchers attempted to present the near-periodic nature of jumping forces by using probability density functions to generate the jumping frequency and Fourier coefficients of each pulse.[14,15] A cosine-squared function was used to generate jumping forces, and the variations in timing were further related to variations in amplitudes of the jumping pulses yielding near-periodic ground reaction forces signals.[16–18] But another researcher pointed out that the symmetric half-sine pattern cannot reflect the asymmetric shapes of the real measured jumping forces. Because, individual jumping should be described as a near-periodic stochastic process rather than a deterministic process. So, a mathematical model to generate stochastic synthetic vertical jumping forces using closed-loop trajectories through a three-dimensional space was developed. The trajectories replicate different sizes and shapes of the measured jumping pulses via a sum of Gaussian exponentials. Their model can represent temporal and spectral features of real human vertical jumping loads more effectively than half-sine pulses and Fourier series models.[19–21]

In China, some other researchers proposed that the real jumping force could be fitted well by a half-sine function for low jumping frequencies, but for high jumping frequencies, the jumping pulse could be better fitted by a half-sine-squared function. Furthermore, in Chen's jumping model, the jumping frequency, contact ratio, and peak factor were considered as random variables. However, the shapes of the jumping pulses are complex and cannot be modeled using only a half-sine or half-cosine function.[22–28] Also, a stochastic approach for generating individual jumping loads considering different jumping force patterns was presented.[29]

However, these models involve complex parameters, and the statistical distributions of their core variables differ substantially from one another. It is not very convenient to use in practice because the formula adopted is complicated. Hence, a stochastic approach for generating jumping loads that is easy to implement in engineering and reflects the real characteristics of jumping forces should be further developed.

This paper aims to investigate jumping load models for spectators and analyze the key parameter characteristics of jumping loads relevant to large-scale temporary grandstands.

To explore the jumping load calculation model and develop a safe and effective load simulation method for large-scale temporary structures, this paper conducts experiments in which eight subjects jumped at frequencies ranging from 1.0 Hz to 3.0 Hz, with measurements obtained directly using a three-axis force plate. In addition, 20 subjects performed jumps on a large-scale temporary grandstand. The experimental results were also used to identify mechanical models describing both the effect of spectators on the grandstand and the response of the grandstand to human loading.[30–32] Also, the most effective arrangement of bracing system for a typical example of the temporary steel grandstand which is exposed to dynamic load induced by spectators was determined.[33]

Based on the test data, a new calculation model of the jumping load was developed. This paper is divided into four parts: first, the subject jumping test process is introduced; second, the core parameters of jumping loads are analyzed; third, a vertical jumping load calculation model is proposed based on the experimental data; and finally, the horizontal load components are discussed, followed by conclusions.

Jumping load tests

In order to accurately analyze the impact of load coupling effects on the core parameters of the individual jumping loads, and in consideration of the similarity between single-person and multiple-person jumps, both single-person and two-person

Figure 1. A grandstand collapsed due to jumping spectators. (https://www.bilibili.com/video/BV1RrK6zMESi/?vd_source=156cd4cd2e8750e749736923f801e9f2)

Table 1. Basic information about subjects.

Number	1	2	3	4	5	6	7	8
Mass (kg)	110.5	73.5	59.5	55.7	81.4	48.5	51.3	115.7
Height (m)	1.90	1.80	1.78	1.70	1.73	1.62	1.60	2.03
Age (year)	26	26	27	23	28	26	25	38
Sex	Male	Male	Male	Male	Male	Female	Female	Male

jumping tests were the main design focus. The tests were preceded by a rigorous risk assessment and received approval from the university's research ethics committee. For subject selection, a large number of actual observations and video recordings indicated that jumping spectators are primarily young adults. Taking into account the most unfavorable combination of spectator load, eight young adults were selected as the test subjects to represent grandstand spectators, based on a rigorous health screening and assessment. Their physical characteristics are listed in Table 1. All eight subjects participated in single-person jumping tests, and a subset of them also took part in two-person jumping tests. The two-person jumps were divided into three groups: Group 1 (Subjects No. 2 and No. 4), Group 2 (No. 4 and No. 5), and Group 3 (No. 5 and No. 6).

Due to different performance events taking place in the stands, such as football matches, audience members may be oriented facing forward, or with their backs to the field; there may also be situations where they are back-to-back or face-to-face with one another. To fully simulate load coupling behavior during jumping, and in consideration of the fact that the body orientation during jumping may have a greater impact on coupled loading, the two-person jump test included two main jumping postures, back-to-back (Figure 2(d)) and facing the same direction (Figure 2(e)). And in this paper, it is assumed that facing forward and having one's back to the field are considered the same, and that being back-to-back and face-to-face are also regarded as equivalent. These same subjects also participated in swaying tests, the results of which are reported in another study.[32] Impact frequency has a great influence on both the jumping load and the vibration response of the temporary grandstand. In order to approximate the jumping behavior of spectators in real scenarios, and in combination with known ergonomic jumping frequency range,[34,35] the test jumping frequencies were controlled within the range of 1.0 Hz–3.0 Hz. For single-person tests, the jumping frequency was gradually increased by 0.1 Hz. For two-person tests, frequencies of 1.5 Hz, 2.0 Hz, 2.5 Hz, and 2.2–3.0 Hz (in 0.2 Hz increments) were selected. A metronome was used to guide the jumping pace. Each test condition was performed twice and followed a standard protocol: the subject stood still on the force plate for weighing, then began jumping in time with the metronome for 20 s(s) with the middle 15 s used for analysis), and finally stepped off the force plate to rest. Considering different plate surface stiffness may influence the natural variability of the jumping load, data were collected by three types of force measurement systems: a single Hur Force Platform (Finland HUR Labs), a Kistler 9287CA force plate (Switzerland), and a wire dynamometer insole. These are illustrated in Figure 2(a–b, c–e, and f–g, respectively). All forces were sampled at 1 kHz to minimize the errors due to time-domain data truncation.

A large number of tests have shown that the formation of a consistent jumping load from spectators takes approximately 15 s; beyond this duration, subjects begin to experience a significant decline in physical performance and enter a state of fatigue, resulting in a progressive reduction in impact forces. To collect effective jumping load data, and in consideration of the sampling theorem, the data acquisition time was set to 10 s, based on a comparison test of different acquisition durations during single-person jumping. Figure 3 shows the raw time-history curve of the vertical load generated by a single subject jumping at 2.0 Hz for 10 s.

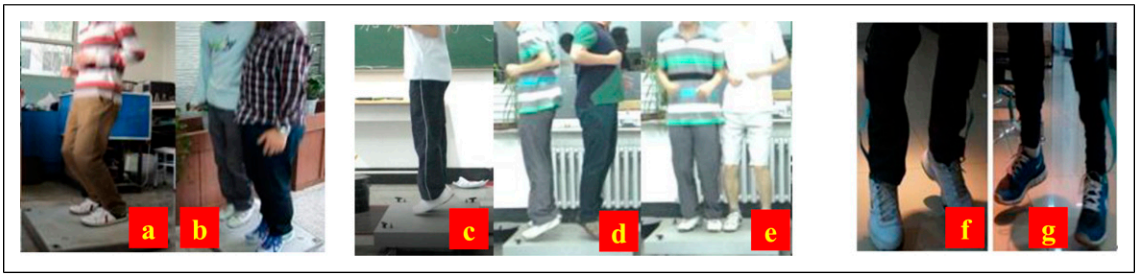

Figure 2. Measured jumping loads with force instruments.

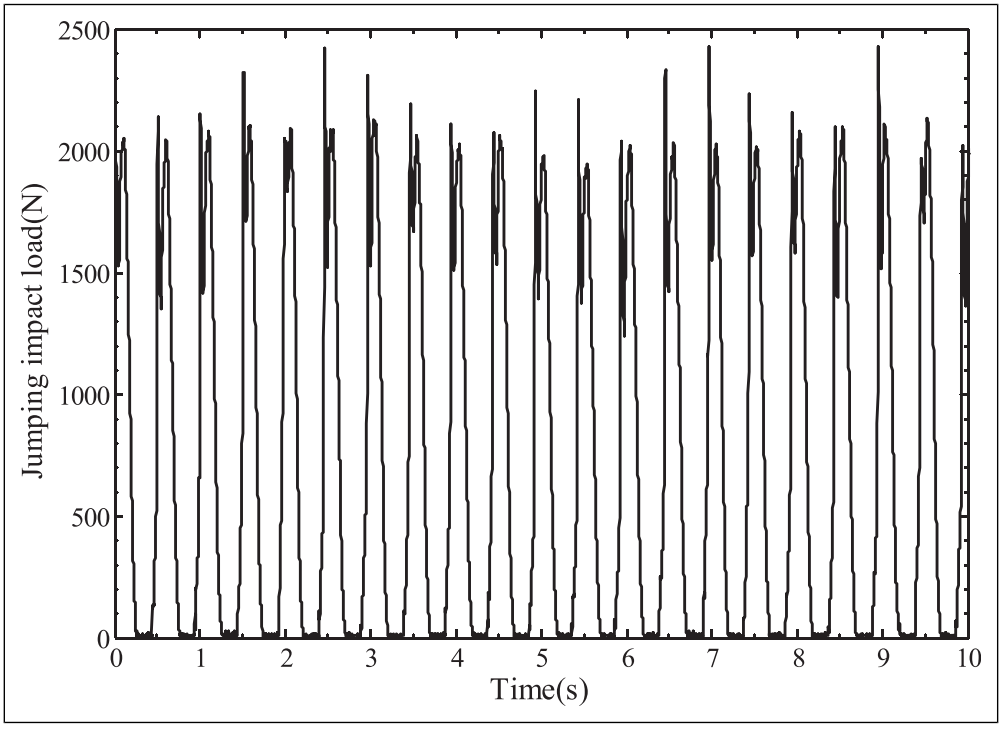

Figure 3. Load time-history curves generated by single subject jumping at 2.0 Hz for 10 s.

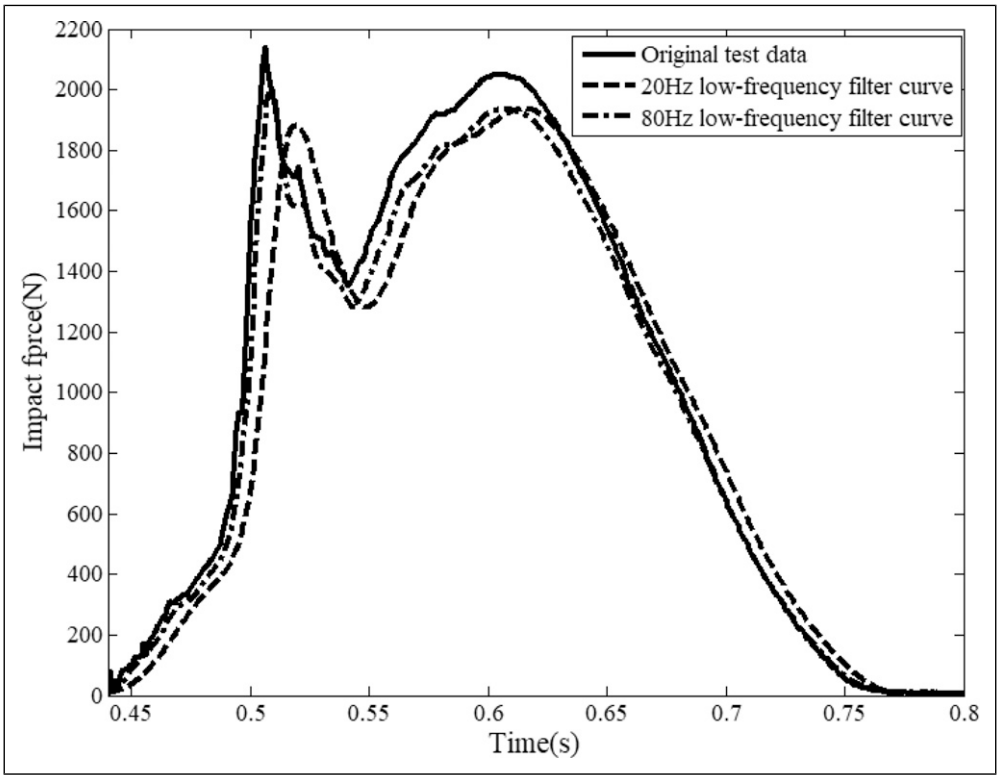

Figure 4. Test data filter.

Test results analysis

Test data preprocessing

Because the process involves low-frequency signal acquisition, the vibration of other structures in the test may introduce noise into the recorded data. In order to improve the signal-to-noise ratio, and in consideration of the jumping characteristics of subjects as well as the need for effective extraction of low-frequency signals during the latter part of the impact contact phase, a low-pass filter with a cut-off frequency of 20 Hz was applied (Figure 3). The curve in Figure 4 shows the load generated by a single jump. Compared with the original impact curve and the filtered result at 80 Hz,[19] the post-processing data represented by the dashed line curve is more suitable for characterizing the subject's behavior: the peak value is better preserved, the curve continuity is improved, and the shape more closely resembles the actual load transition process. After filtering, a total of 333 valid data records were obtained.

In this paper, the subject's impact load curves exhibit three distinct shapes: single-peak, near-single-peak, and double-peak forms. Figure 5 illustrates the evolution of these curve characteristics as two subjects jump at frequencies ranging from 1.0 to 3.0 Hz. The superimposed curves in this figure represent a large number of single-person jump load data points. Analyzing the trends in curve shape, it can be concluded that double peaks primarily occur during low-frequency jumps; near-single-peak curves are most common in the 1.5–2.5 Hz range; and single peaks dominate in the 2.0–3.0 Hz range. The major cause of these waveform differences is the variation in contact time between the subject and the force plate. During double-peak low-frequency jumps, the contact time is longer; at this stage, the knees bend after landing, and the soles of the feet maintain full contact with the plate. When the frequency exceeds 2.0 Hz, subjects' jumping motions vary noticeably. To maintain continuous take-off, the subject's soles are no longer in synchronized contact with the plate. Some subjects maintained full sole contact, while others transitioned to earlier toe contact, causing the waveform to shift from a double peak to a single peak, thus generating the near-single-peak and single-peak forms. However, by 2.7–3.0 Hz, all subjects were observed to contact the plate exclusively with their toes. For example, Figure 5(a) shows that Subject No. 5 transitioned from full sole to toe contact after the frequency surpassed 1.9 Hz, with the curve evolving from double to single peak. Figure 5(b) displays the waveform for Subject No. 2, who maintained full sole contact below 2.7 Hz. At 3.0 Hz, the waveform transformed fully into a single peak. Based on this data, the study categorizes jumping impacts into two types based on contact time: "partial sole contact" and "full sole contact." Subjects No. 4 and No. 5 belong to the partial sole contact group (left side of Figure 5(c)), while the other six subjects belong to the full sole contact group (right side of Figure 5(c)). These two contact types correspond to different frequencies and require distinct impact load models.

Load characteristic parameters

The spectator jumping load is a typical random dynamic load, influenced by many uncontrollable variables. However, experiments[18] have shown that three key parameters play a dominant role: load peak ratio k_p (where p denotes peak value), defined as the ratio of the peak value of the impact load curve to the weight of a single subject; jumping period T_s (s denotes single time of one jump), defined as the time interval from one downward crossing of the zero load level to the next; and contact time T_c (c denotes contact time of one jump), defined as the time duration for which the subject remains in contact with the ground during each jump. Figure 6 illustrates the physical meaning of these three characteristic parameters. In the figure, $F_{max,i}$ represents the peak force generated during the i-th jump, and G denotes the subject's weight. Because these parameters directly reflect the variation and structure of the jumping load curve, the following sections provide a detailed analysis of their behavior based on the experimental data.

Load peak ratio k_p. k_p is an important indicator that measures the magnitude of impact energy generated by a jumping subject. In various countries, existing crowd load calculations are based on human body weight distribution. When combined with the k_p distribution observed in experiments, these models provide estimated standard load values. For example, BS6399[5] and [NBCC][9] recommend a value of 4.8 kPa. However, there is currently no specific calculation method for jumping loads on temporary structures. Some regional standards simply adopt a fixed value of 3.5 kPa,[36] derived from general crowd load codes, but without sufficient empirical justification. Because jumping loads are highly frequency-dependent random loads, determining a reasonable k_p value under given frequency conditions is not only essential for accurate load prediction, but also plays a critical role in structural optimization and resonance avoidance. Each subject tends to have a personal k_p distribution range (Figure 7). Figure 7(a) shows the k_p distribution for Subject No.2. The scatter points indicate k_p values at different jump frequencies, while the star-shaped markers denote average values. The data show that both k_p values and averages vary across frequencies for the same individual. Figure 7(b) compares the average k_p trends for

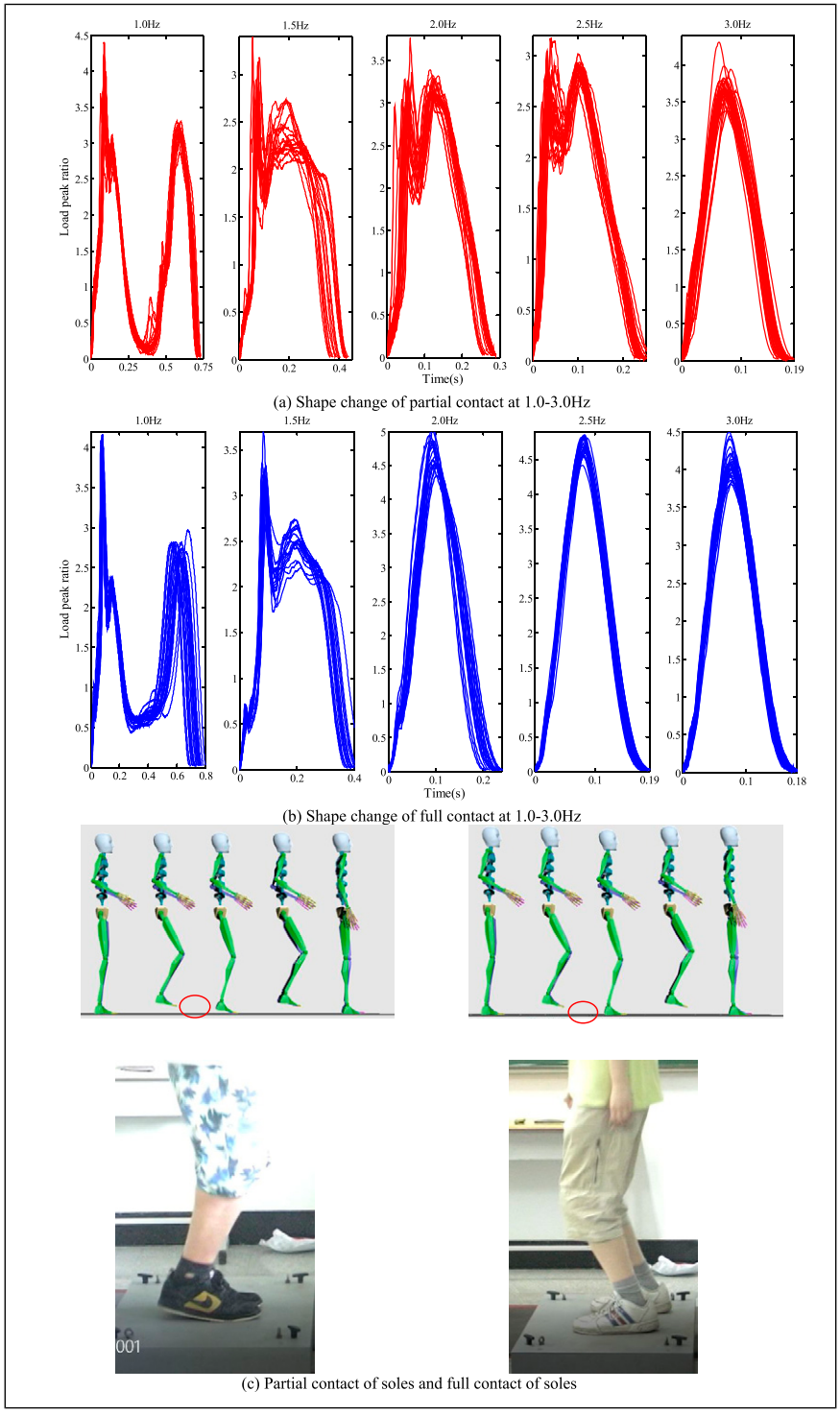

Figure 5. Curve of jumping load.

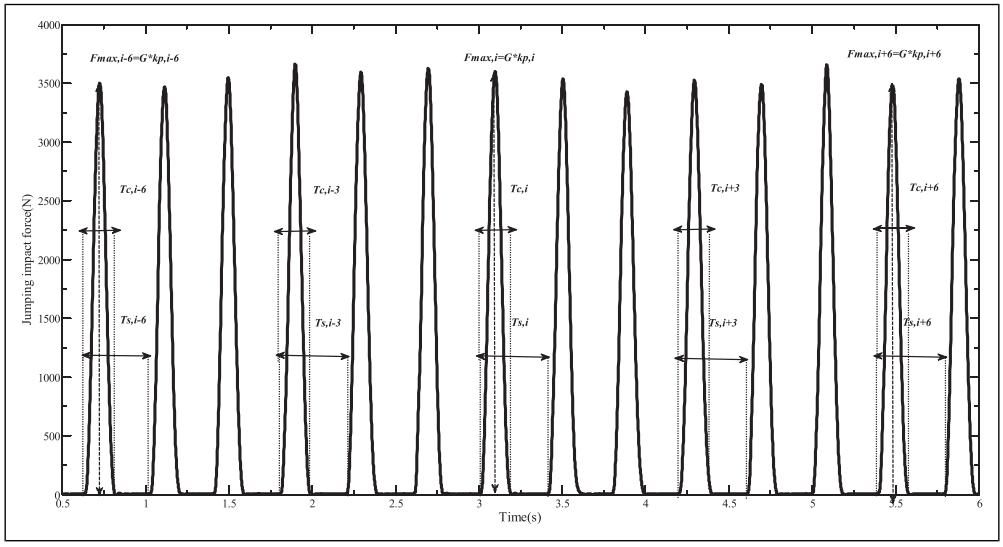

Figure 6. Characteristic parameters of the force signal.

different subjects. or those in the partial sole contact group (represented by pink and black curves), k_p values tend to increase initially and then decrease with increasing frequency. This suggests optimal jumping performance and maximum impact energy within a particular frequency band; at higher frequencies, delays in jumping lead to reduced k_p values. For the full sole contact group (Subjects Nos. 1, 2, 3, 6, and 7), although the contact mechanics differ, the trend is generally similar. However, the k_p magnitudes differ. Specifically, when the jumping frequency exceeds 1.7 Hz, the full contact group tends to have higher average k_p values than the partial contact group. Figure 7(c) presents the distribution of 6035 k_p values across all subjects. Blue dots represent average values, and the red dots show variance. The variance peaks at 2.3 Hz, with a value of 0.56, indicating that jumping impact loads become more dispersed and less predictable at higher frequencies.

According to the above analysis, directly using the average value of k_p to simulate the jumping load introduces significant error and fails to capture the variability of k_p from one jump to the next. Based on the k_p variance shown in Figure 7(c), it is evident that incorporating a residual component can better represent the fluctuation characteristics of the peak ratio. This leads to the formulation shown in equation (1):

$$k_{pi} = \bar{k}_{pi} + \Delta k_{pi} \tag{1}$$

where k_{pi} represents the peak value generated by the jump i, $\bar{k}_{pi}$ represents the average value of all jump peak ratios at a certain jumping frequency, and Δk_{pi} represents the residual.

The K-S (Kolmogorov–Smirnov) hypothesis test (using the kstest function in MATLAB) was performed on the variables formed by the residuals $\Delta k_{pi,}$ and the results showed that these residuals follow a normal distribution (Figure 8(a)). From the figure, it was observed that the data deviate significantly at both ends of the distribution. After applying truncation correction, the probability distribution curve at each frequency was calculated, as shown in Figure 8(b). Using a 95% confidence level, the normfit function in MATLAB was used to determine the confidence interval corresponding to each jumping frequency Δk_{pi}, based on the Monte Carlo method and combined with the truncated normal distribution. The normrnd function was used to generate random variable intervals that conform to the observed statistical characteristics. These randomly sampled Δk_{pi} values were then inserted into equation (1) to compute individual k_{pi} values. This approach provides a quantitative method for simulating the peak ratio of each subject's jumping load based on experimentally derived distributions.

T_s and T_c. The parameters T_s and T_c have a significant impact on the characteristics of the jumping load and the vibration behavior of the temporary structure. In consideration of the load amplitude coverage, it was stipulated that a load value greater than 15 N is treated as the start of a load event, while any value less than 15 N is treated as zero load. According to the above definitions, a total of 11,214 measured values of T_s and T_c were obtained. Figure 9(a) shows the distribution of T_s and T_c values. It can be observed from the figure that both T_s and T_c decrease gradually as the jumping frequency increases. A comparison between the average T_s for six subjects and the test period (the reciprocal of the metronome control frequency) is shown in Figure 9(b). The maximum square sum of deviations of the measured period was found to be 7.8×10^{-4} at 1.3 Hz,

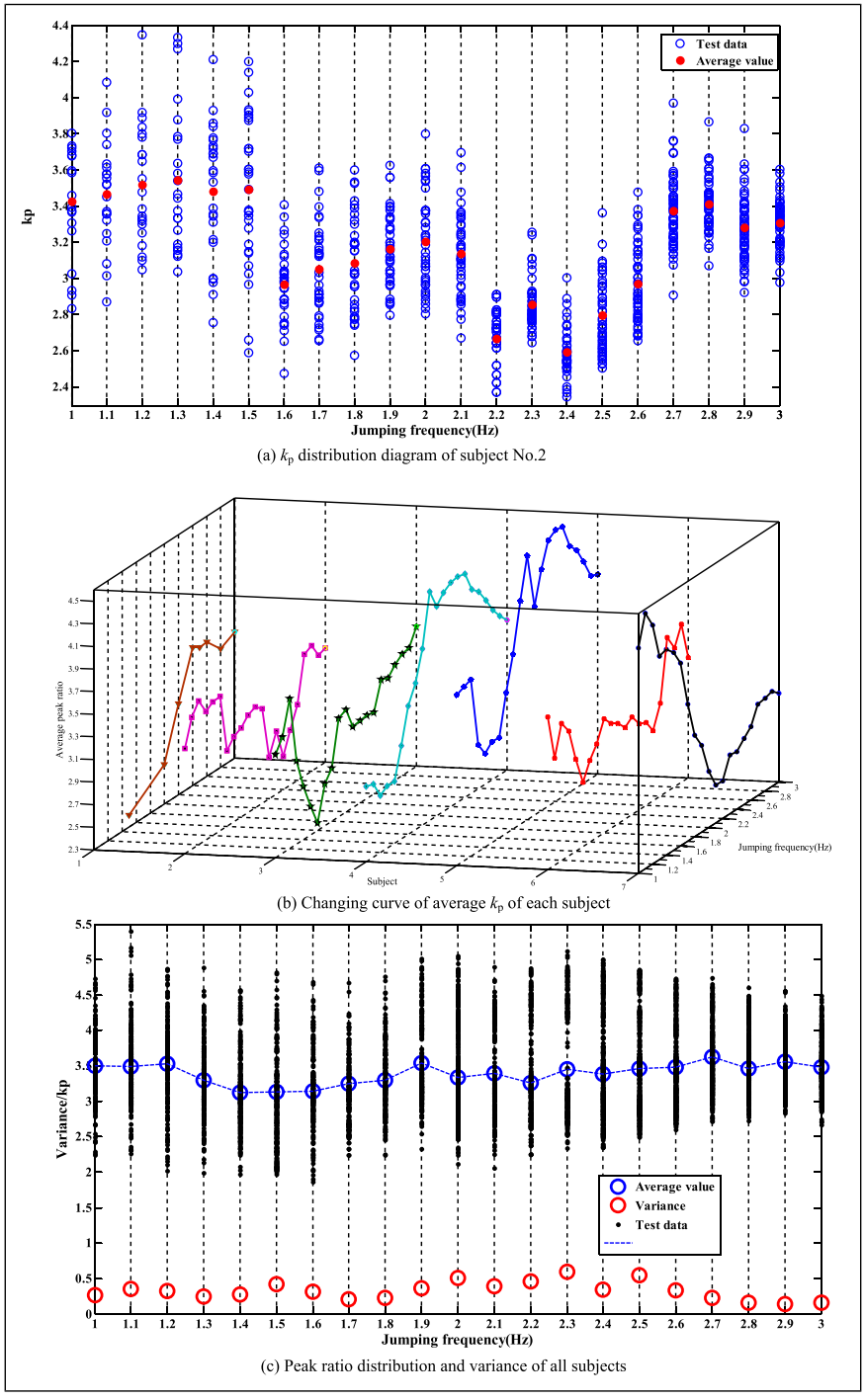

(a) k_p distribution diagram of subject No.2

(b) Changing curve of average k_p of each subject

(c) Peak ratio distribution and variance of all subjects

Figure 7. Distribution of k_p.

which represents only 0.1% of the test period. This indicates that the average measured T_s is close to the test period. In contrast, Figure 9(c) shows the variation in average T_c across subjects. The largest square sum of deviation is 0.026 at 1.8 Hz, which represents 7.6% of the total average. This suggests that the variability in T_c across different subjects is significantly greater than that in T_s. This distinction arises because, during testing, subjects can regulate their take-off timing in synchrony with the metronome, resulting in a stable T_s. However, the ascent and descent phases after take-off are influenced by random body motion, leading to substantial differences in T_c among individuals.

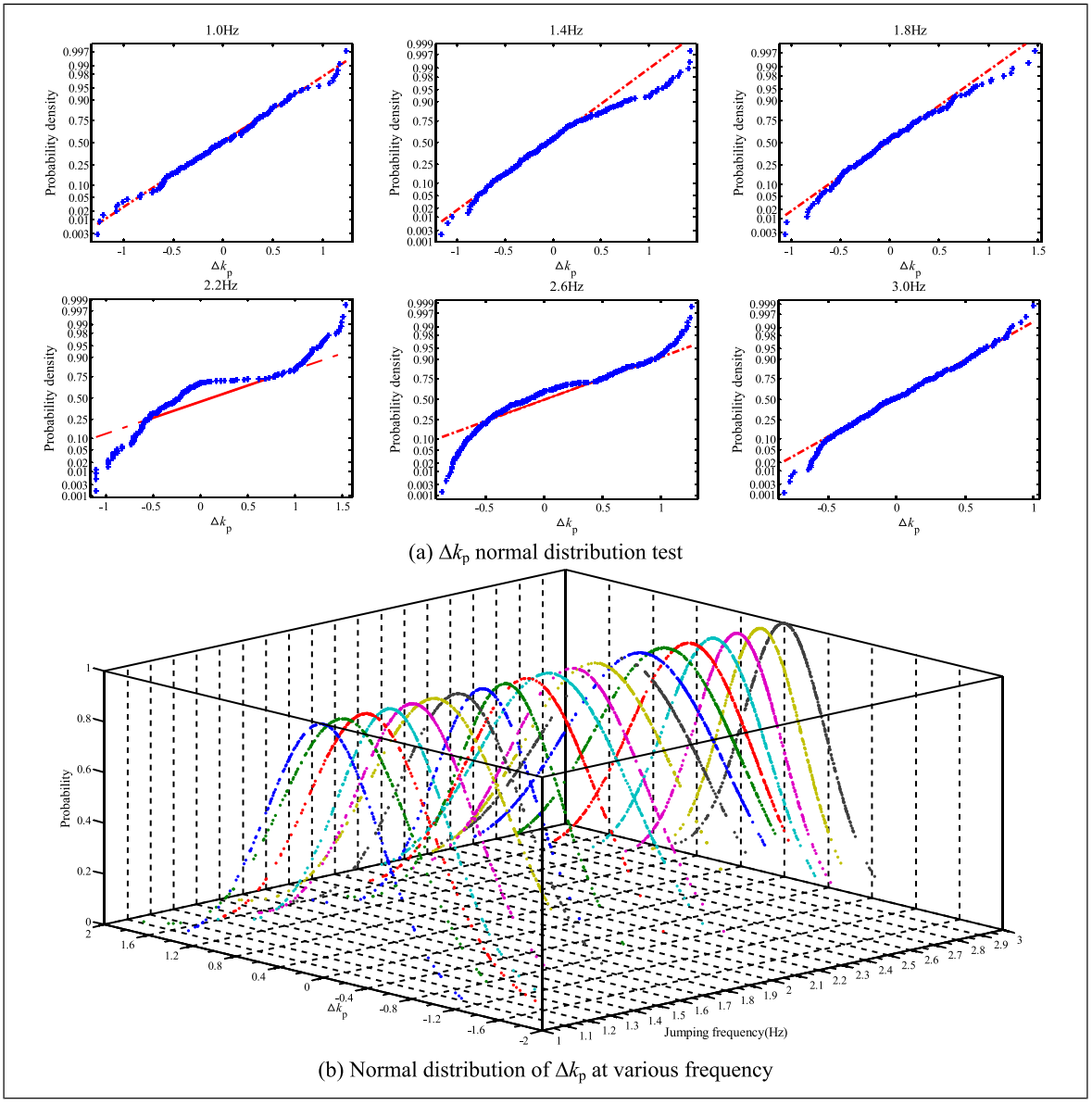

Figure 8. Normal distribution of Δkp.

A parameter derived directly from T_c and T_s, is the jumping contact ratio, denoted as α, and defined as T_c/T_s.[11] The relationship between α jump frequency f was calculated based on the average values of T_c and T_s for all subjects, as presented in Figure 9(b) and (c). This relationship is illustrated in Figure 10, which shows how the contact ratio varies with jumping frequency.

From the left panel of Figure 10, it can be seen that as jumping frequency increases, α first decreases and then increases, reaching a minimum value of 0.58. This minimum is notably higher than the 1/3 value typically associated with normal jumps, as proposed by T. Ji,[11] and is broadly consistent with values greater than 0.5 reported by Sim[18] and Racic.[21] This indicates that subjects maintain a relatively long contact time during jumping, which in turn means that the load acts on the structure for a longer duration. This extended contact time is unfavorable for structural stability and increases the risk to spectator safety. The polynomial expression describing the relationship between α and frequency f was derived using a nonlinear least-squares fitting method. In the right panel of Figure 10, the relationship between T_c and T_s is also analyzed.

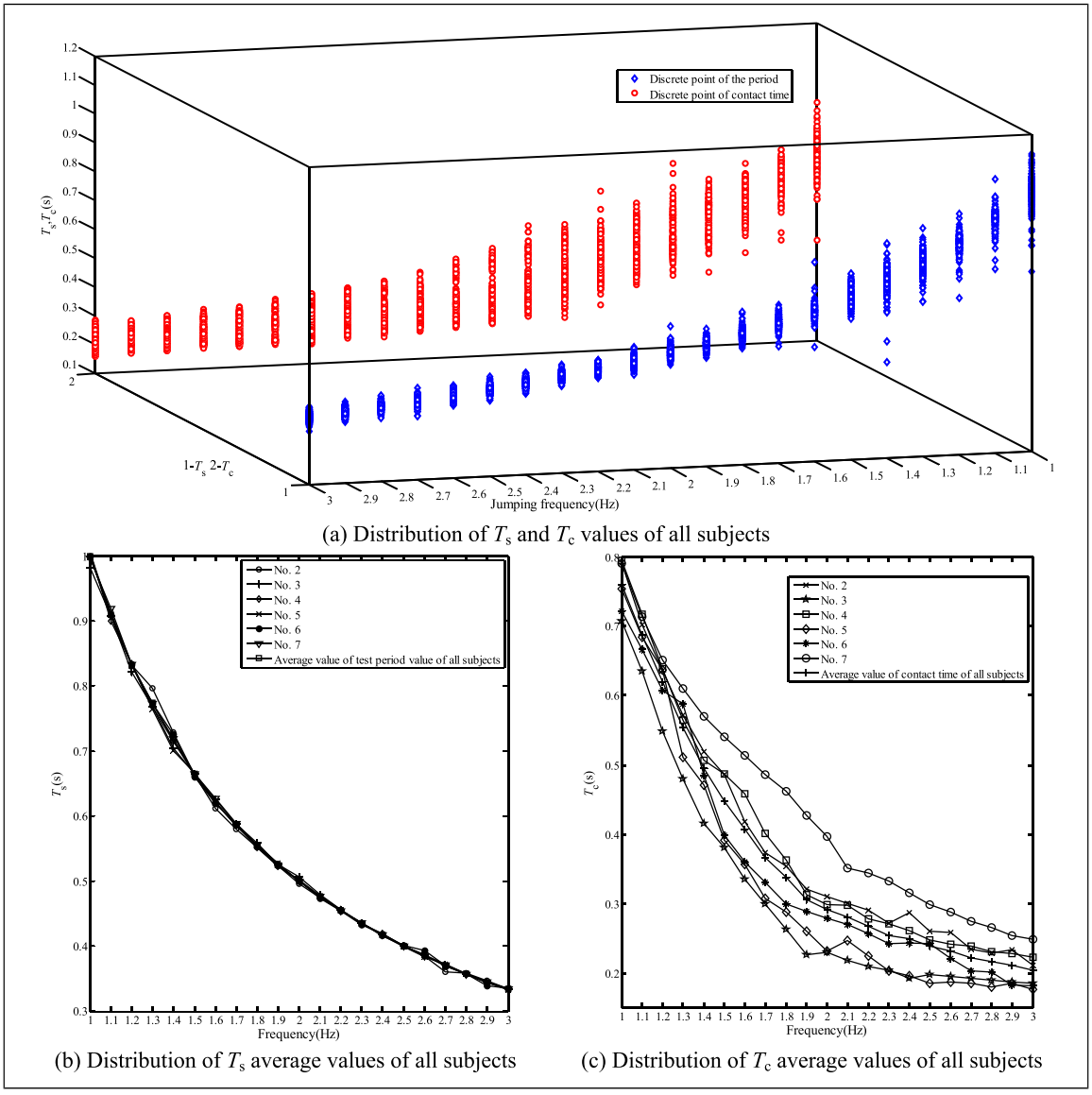

(a) Distribution of T_s and T_c values of all subjects

(b) Distribution of T_s average values of all subjects

(c) Distribution of T_c average values of all subjects

Figure 9. The distribution of T_s and T_c.

This figure illustrates the T_s (ranging from 1.0 to 3.0 Hz) and T_c as a holistic dataset, which appears to exhibit a linear relationship on the graph. However, when analyzed at each individual jumping frequency, it becomes evident that not all T_s and T_c demonstrate a linear relationship, this is precisely what we analyze in Figure 13 later on.

To better reflect the variations in T_c and T_s across different jumps by the same subject and among different subjects, and to make the simulated timing parameters more representative of the actual behavior, a residual-based modeling approach was used, similar to the method for k_p in the previous section.

$$T_{si} = \overline{T}_s + \Delta T_{si} \tag{2}$$

where T_{si} represents the jumping period of the jump i(s), $\overline{T}_s$ represents the average value of the jumping periodic(s), and ΔT_{si} represents the period residual of the jump i(s).

Using the same method, the contact time residual can be defined as shown in equation (3):

$$Tci = \overline{Tc} + \Delta Tci \tag{3}$$

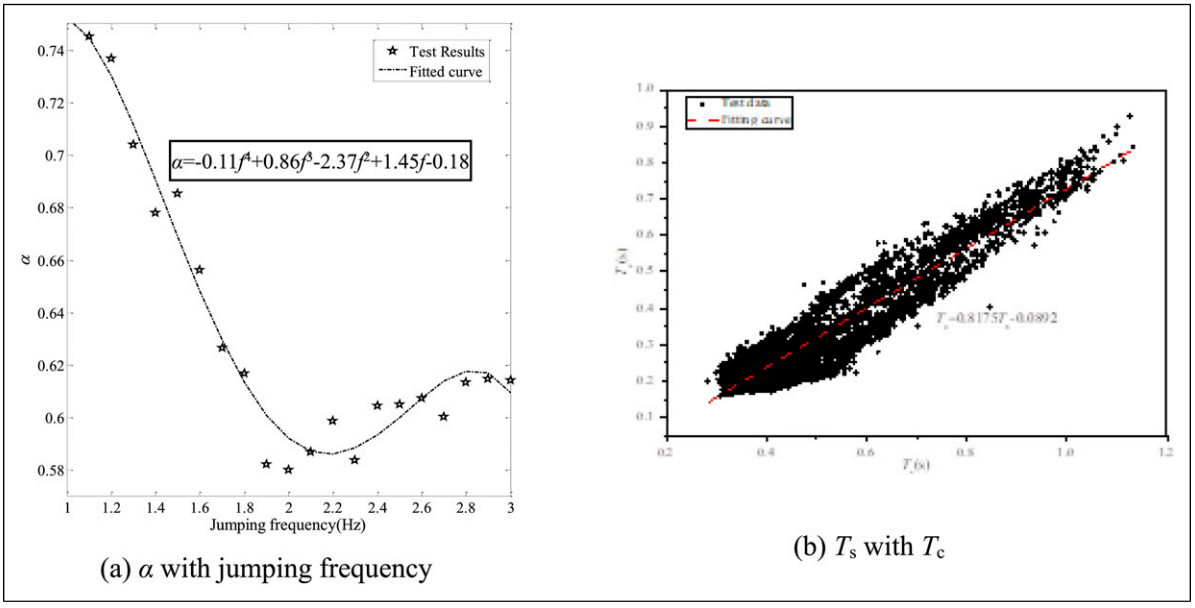

Figure 10. Relationship curve between α and f (T_c and T_s).

where T_{ci} is the contact time for the i-th jump(s), ___T_c is the mean contact time(s), and ΔT_{ci} is the residual for that specific jump(s). Similar to the residual analysis performed for Δk_{pi}, K-S hypothesis tests were applied to the residuals $\triangle T_{si}$ and ΔT_{ci}, as shown in Fig. 11(a). The data were also processed using truncated normal distribution fitting, with results presented in Figure 11(b) and (c). At each jump frequency, the confidence intervals and variation ranges for ΔT_{si} and ΔT_{ci} were computed. Random values for ΔT_{si} and ΔT_{ci} can then be sampled from these intervals and substituted into equations (2) and (3) to reconstruct simulated values that match the observed statistical behavior.

Parameter correlation. In order to further clarify whether k_p, $T_{s,}$ and T_c are correlated to each other, the first step was to analyze the relations between k_p and T_s and between k_p and T_c at the intrasubject and at the intersubject levels, respectively. Figure 12 illustrates these relationships at 1 Hz, 2 Hz, and 3 Hz. It can be seen from the figure that, regardless of whether the comparisons were made within the same subject (intrasubject) or across different subjects (intersubject), the correlation coefficients between these parameters were generally less than 0.5. Further analysis across additional frequencies also indicates that no direct linear correlation exists between k_p, $T_{s,}$ and T_c.

Secondly, the relation between T_s and T_c at both the intrasubject and intersubject levels was also analyzed. As shown in Figure 13, with the exception of a clear linear relationship between T_s and T_c at 1 Hz, there is no significant linear correlation between them at other frequency bands. In addition, it is observed that although one subject initially exhibited a linear relationship between T_s and T_c across all jumping frequencies, the strength of this relationship decreased rapidly as the frequency increased. This further confirms that there is no consistent or obvious linear correlation between T_s and T_c.

In summary, the three basic characteristic parameters are statistically independent, and through equations (1–3), the jumping load characteristics, peak ratio, jump time, and contact time, are expressed in terms of a unified framework of residuals and frequency. This formulation lays a solid foundation for developing a comprehensive calculation model of the jumping load.

Single-person vertical load simulation

Aiming at the load curve shapes, both single-peak and non-single-peak types observed among subjects, and based on the distribution of the jumping load characteristic parameters and their relationships with frequency and residuals, a quantitative simulation model was developed.

For the single-peak case, the load is assumed to be a periodic symmetric curve, with the cosine function[16] used as the primary basis of the jumping load model. To accurately represent the characteristics of the jumper's load within the cosine model, the peak curve is computed using the subject-specific characteristic parameters adjusted by residual correction, as shown in equation (4):

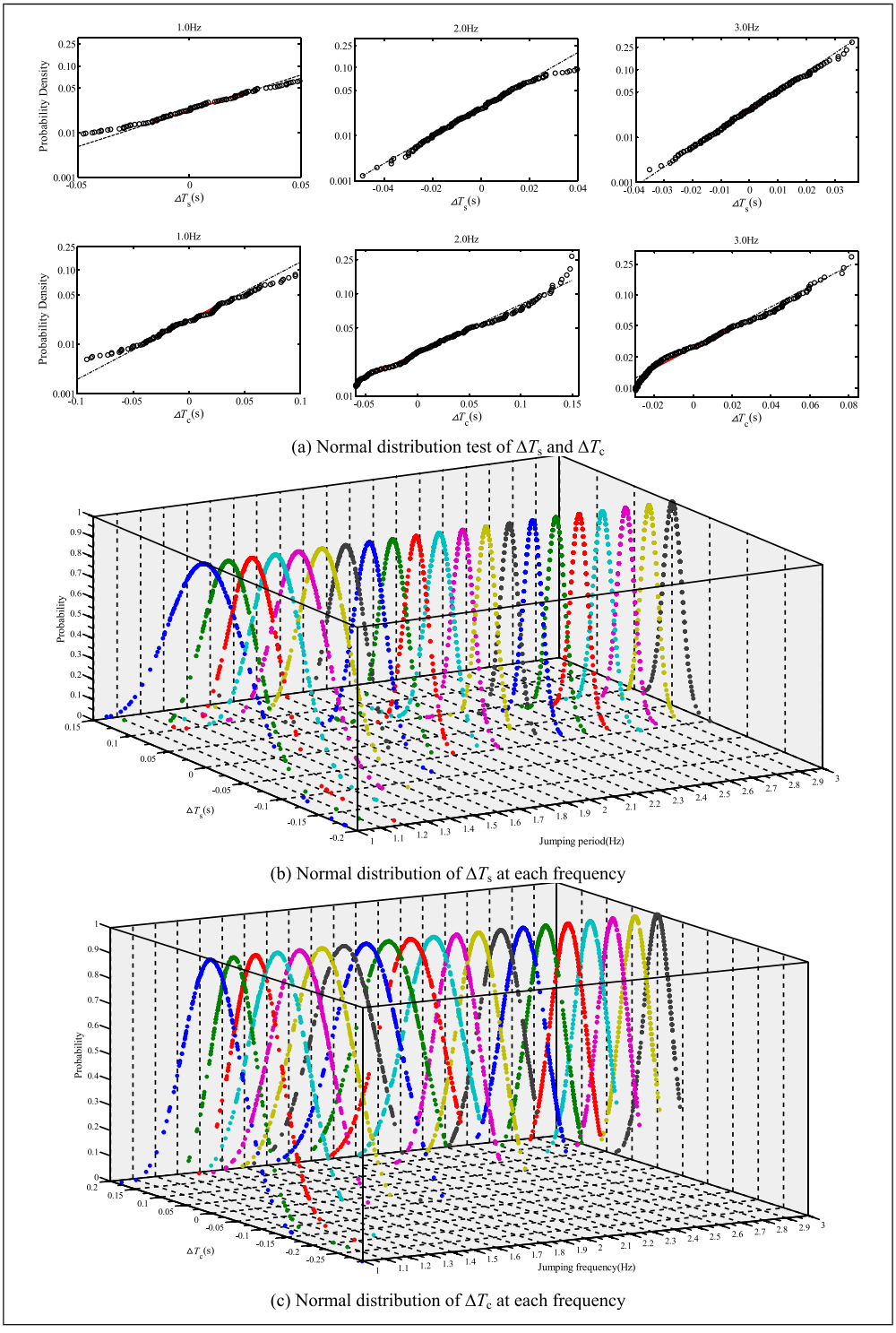

(a) Normal distribution test of ΔT_s and ΔT_c

(b) Normal distribution of ΔT_s at each frequency

(c) Normal distribution of ΔT_c at each frequency

Figure 11. Normal distribution of ΔTs and ΔTc.

$$F_{si}(t) = k_{pi}\cos^2[\pi/T_{ci}(t + T_{ci}/2)], t \in [0, T_{ci}];\ F_{si}(t) = 0, t \in [T_{ci}, T_{si}] \tag{4}$$

where $F_{si}(t)$ represents the dimensionless load value for the i-th jump; t is the time variable within a single jump cycle(s); k_{pi}, $T_{si,}$ and T_{ci} are calculated according to equations (1–3), respectively.

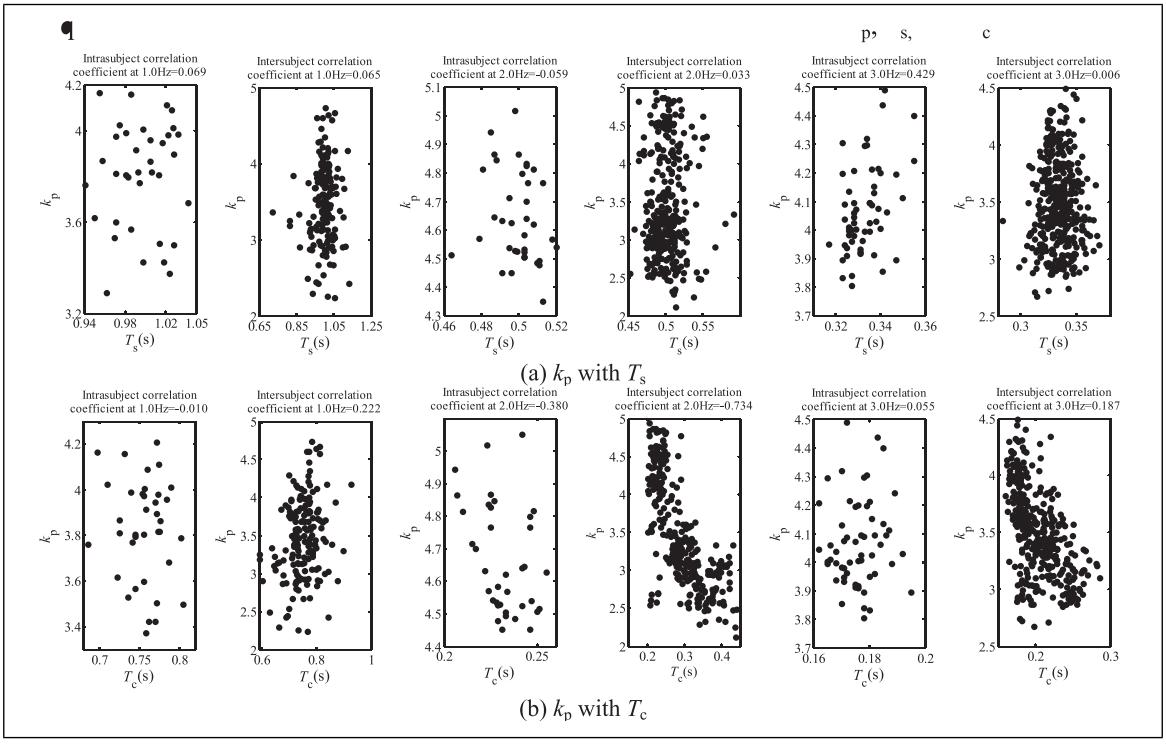

Figure 12. k_p with T_s and T_c at intrasubject and intersubject.

In order to test the reliability of equation (4), and without loss of generality, a jumping frequency of 2.5 Hz, which was relatively easy to maintain, was selected for the comparison test. Equation (4) was used to simulate the single-peak jumping load at 2.5 Hz, and the resulting curve was compared with the measured test curve (Figure 14). For Figure 14(a), the solid line curve represents the actual measured data, the dotted line curve shows the simulation result from equation (4), Figure 14(b) indicates the error between the simulated and measured values. The calculated standard error of the model is

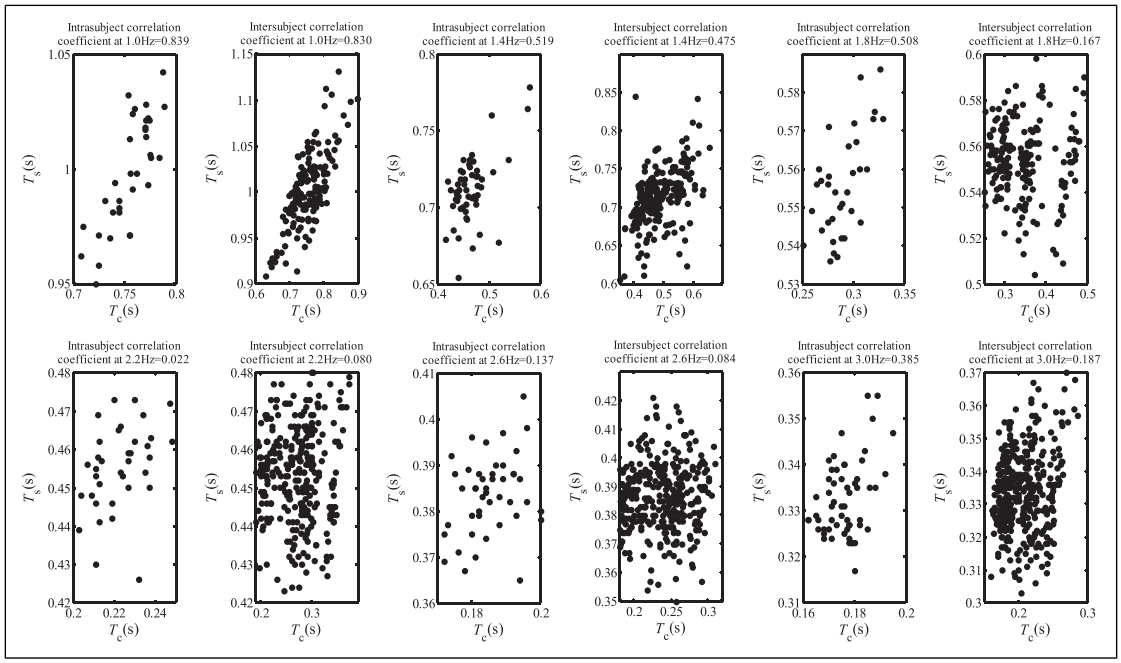

Figure 13. T_c with T_s at intrasubject and intersubject.

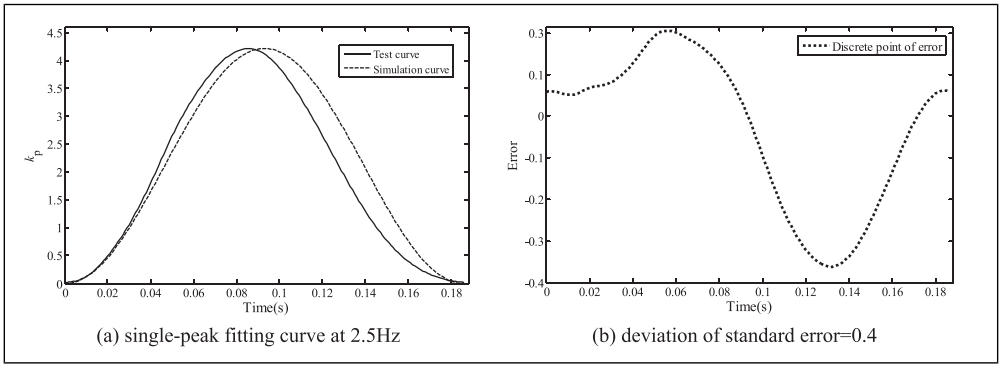

(a) single-peak fitting curve at 2.5Hz (b) deviation of standard error=0.4

Figure 14. Subject jumping load single-peak fitting curve and deviation at 2.5 Hz.

0.4. Considering that the load curve naturally varies with each jump, the simulated jumping shape and load magnitude produced by the model in equation (4) can be considered feasible and representative of actual subject behavior.

For multi-peak load curves, Racic[21] proposed a curve-fitting method based on the Gaussian series and ASD (auto-spectral density) dominant frequency analysis. However, this method requires a high-order Gaussian series, with Racic's model including up to 100 terms, resulting in a significant computational burden. This imposes considerable challenges for real-time calculations and optimization in large temporary structures. Such computational constraints are a key feature that differentiates temporary structures from permanent ones. To address this limitation, the present study combines the calculation of T_{si} and T_{ci} (from equations (2) and (3)) with the Haver Gaussian calculation method[37] to simulate the multi-peak jumping load. The resulting fitting model is expressed as follows:

$$Z_{si}(t) = \sum f_{ij} e^{-[(t-ti j)/bij]2}, t \in [0, T_{ci}]; \; Z_{si}(t) = 0, t \in [T_{ci}, T_{si}] \tag{5}$$

where $Z_{si}(t)$ is the dimensionless load function for the i-th jump; t is the time variable for a single jump cycle(s); f_{ij} is the peak value of the j-th Gaussian component in the i-th jump; t_{ij} is the time location of that peak; b_{ij} is the width parameter of the j-th Gaussian curve in the i-th jump.

When determining the above parameters, the selection of n (the number of Gaussian components) directly affects the accuracy of the curve fitting. According to the observed characteristics of impact curves, the curve becomes more complex as frequency decreases (Figure 5). To meet a relative error threshold of 10%, the Haver Gaussian algorithm was applied using equation (5) as the objective function to fit non-single-peak jumping curves at 1.1 Hz (Figure 15(a)) and 1.5 Hz (Figure 15(b)). In the figure, the blue curve represents the measured data, the red curve shows the multi-peak Gaussian fitting result, and the black curves represent the individual peak components. The green curve indicates the root mean square error

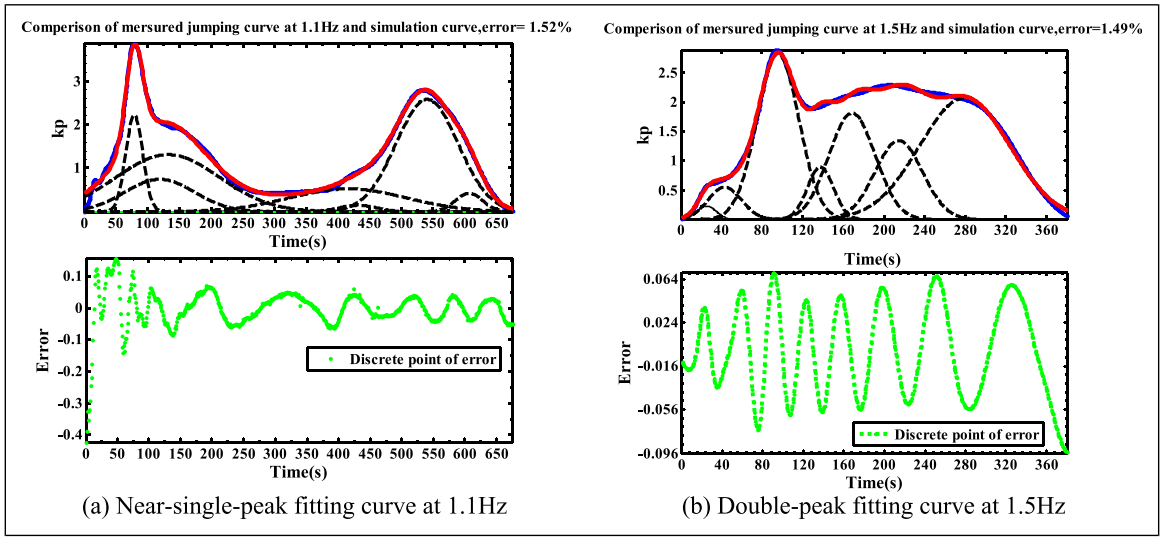

(a) Near-single-peak fitting curve at 1.1Hz (b) Double-peak fitting curve at 1.5Hz

Figure 15. Fitting curve and errors of non-single-peak shape.

(RMSE), which was found to be 1.49% and 1.52% for 1.1 Hz and 1.5 Hz, respectively, demonstrating the feasibility of the model using the Haver Gaussian fitting method. To determine the optimal value of n required to fit all jumping load curves, curves across the frequency range 1.0 Hz–2.6 Hz were repeatedly fitted. The maximum required value of n was 14 (for the 1.0 Hz curve), corresponding to 52 fitting parameters. This is a significant reduction compared to the 100 terms used in the method proposed by Racic.[21] The minimum value of n was 4 (for the 2.6 Hz curve), demonstrating that the proposed method greatly improves the efficiency of simulating low-frequency jumping impact loads. This improvement is of substantial practical significance for on-site load testing of large-scale temporary structures.

Most jumping spectators are young adults, according to the *2020 National Physique Monitoring Bulletin*, have an average weight of 72.475 kg (man aged of 20–59) and 58.85 kg (women aged of 20–59). According to the truncated normal distribution, the weight range for men is estimated to be 70.4–74.3 kg, and for women, 55.7–60.8 kg. Assuming a 95% confidence level and a standard deviation of 20 kg, men's weight is modeled as a normal distribution: G ~ N (72.475 kg, 20 kg), while women's weight follows: G ~ N (58.85 kg, 20 kg). Using these assumptions, the design standard value of the vertical load for jumping by a single spectator can be calculated using equation (6) with MATLLAB software:

$$G \cdot F_{si}(t) = G \cdot Z_{si}(t) = \text{normrnd}(72.475, 20) \text{ for men or normrnd}(58.85, 20) \text{ for women} \quad (6)$$

In order to further enable both automatic calculation of jumping loads and rapid simulation of spectator-induced loads in large temporary structures, the data processing workflow is shown in Figure 16. The main steps include the following: (1) Establishing a parameter database using the three characteristic parameters obtained from experiments along with the multi-peak Gaussian fitting parameters; (2) Selecting the jumping type, including determination of curve shape, jumping

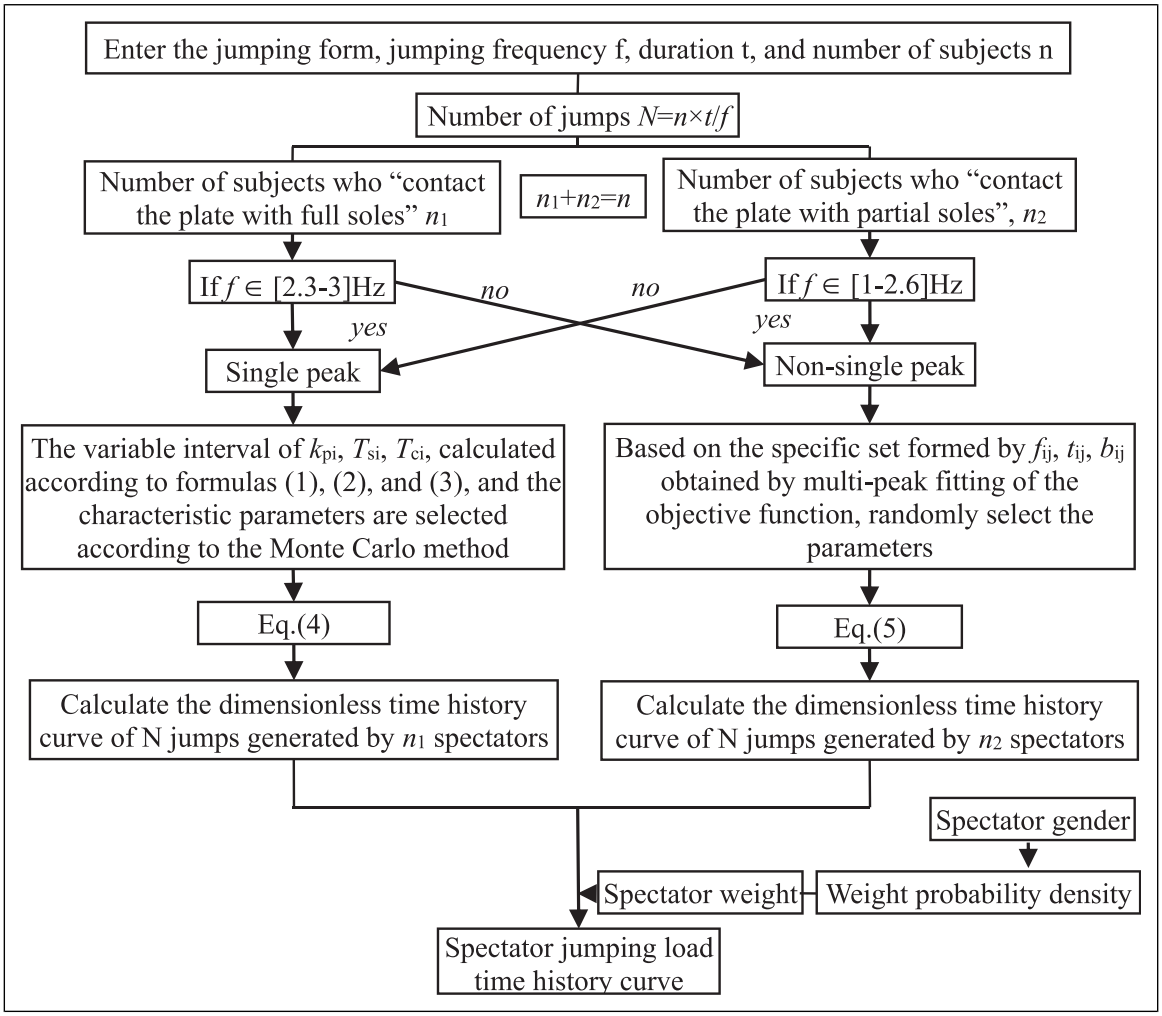

Figure 16. Spectator jumping load algorithm.

frequency, duration, and number of subjects; (3) Retrieving parameters from the database based on the selected curve shape and jumping frequency; (4) Applying the Monte Carlo method to randomly sample parameters; (5) Calculating the jumping load using either equation (4) or equation (5) to obtain normalized load data; and (6) Selecting spectator weights and displaying the load time-history curve.

Above process was coded using MATLAB program developed as shown in Figure 16 (see Appendix I), the vertical load time-history curve of domestic spectators can be automatically simulated over the frequency range of 1.0 Hz–3.0 Hz, for any number of subjects and jump cycles. To verify the feasibility of the program, simulated jumping curves at 1.5 Hz (Figure 17(a)) and 2.5 Hz (Figure 17(c)) were generated and compared with the corresponding measured curves. It can be seen that the simulated curves accurately capture the shape characteristics, exhibit quasi-periodic asymmetry, and are highly similar to the measured data. Further analysis of the amplitude spectra for both simulated and measured curves (Figure 17(b) and (d)) shows that the simulated curves fully capture the dominant frequency components of the measured signals. This demonstrates that the simulation can effectively reconstruct the dynamic impact imposed on the supporting structure during spectator jumping. Such accuracy is crucial for simulating spectator-induced jumping loads and serves as an important

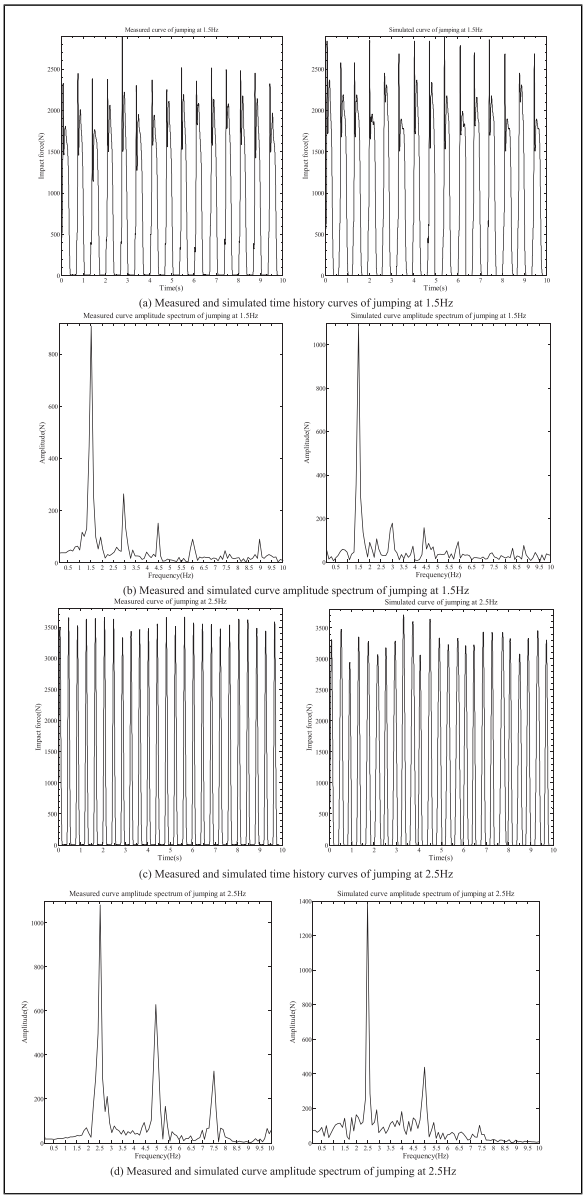

Figure 17. Measured and simulated curve comparison and spectrum analysis.

criterion for evaluating the quality of the simulated curves in reproducing both the vibration and impact effects on the structure.

Impact of jumping mode on spectator load

The characteristic parameters of the load generated by the simultaneous jumping of a large number of spectators are significantly more complex than those of a single spectator, due to the coupling effects of multi-body motions. The low-

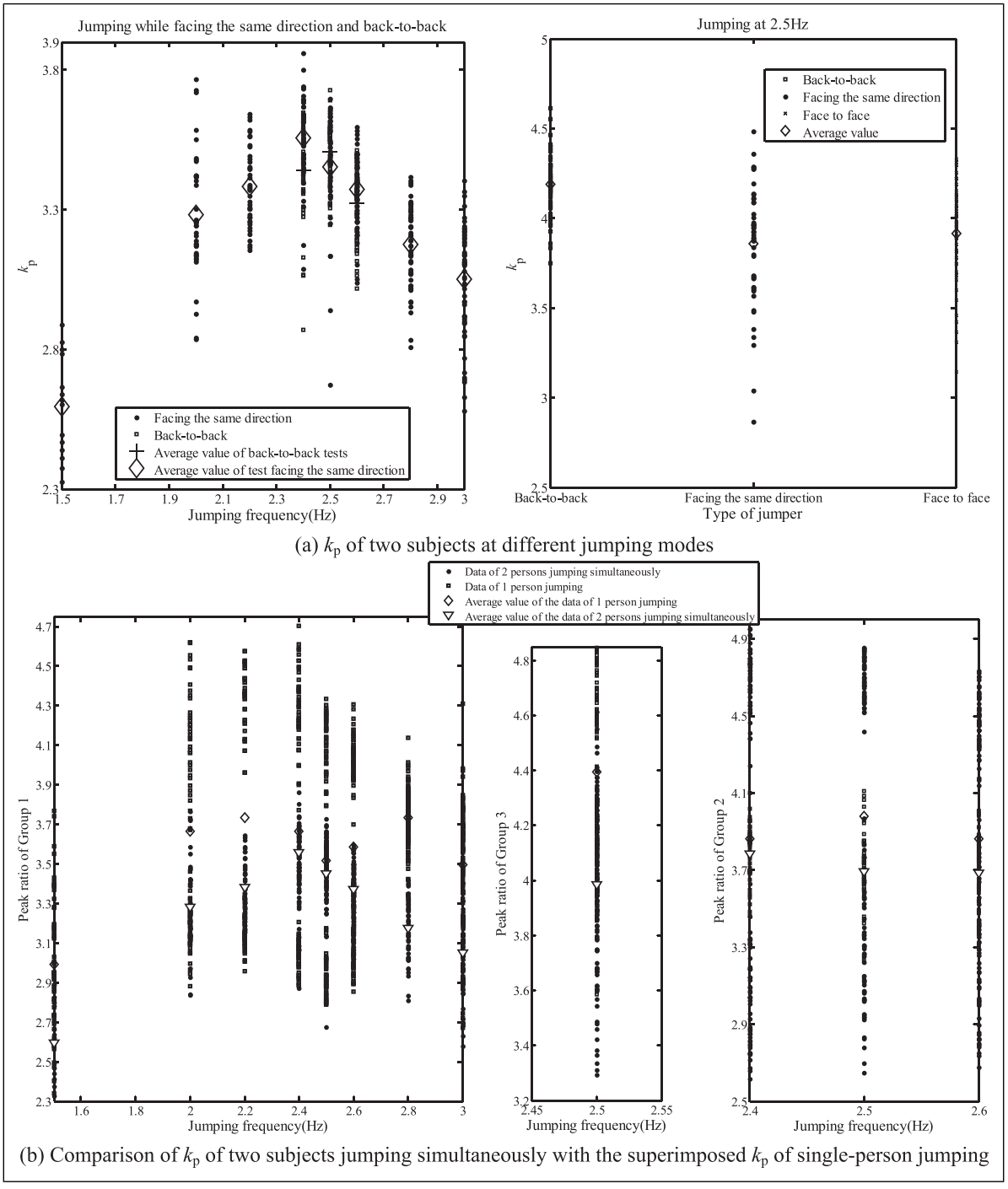

Figure 18. Comparison of k_p of two persons jumping with k_p of a single subject jumping.

frequency characteristics of crowd jumping are also more likely to induce resonance in temporary grandstands. Therefore, effectively determining a calculation model for crowd-induced loads is a critical component in the real-time design and modification of large temporary structures. The two-person jumping load serves as the foundation for modeling larger crowd loads. To investigate the effect of two-person jumping on spectator-induced loads, this section focuses on analyzing changes in the characteristic parameters of the jumping load from the perspective of jump mode, a key step in the development of a reliable crowd load model.

There are many factors that affect the coupling behavior of the spectators during jumping, and one major factor is the variation among individuals. Such differences include IaSV (intrasubject variability) and IeSV (intersubject variability).[21] This paper focuses on the impact of jumping direction (a form of IeSV) on the peak ratio k_p. The most common jumping

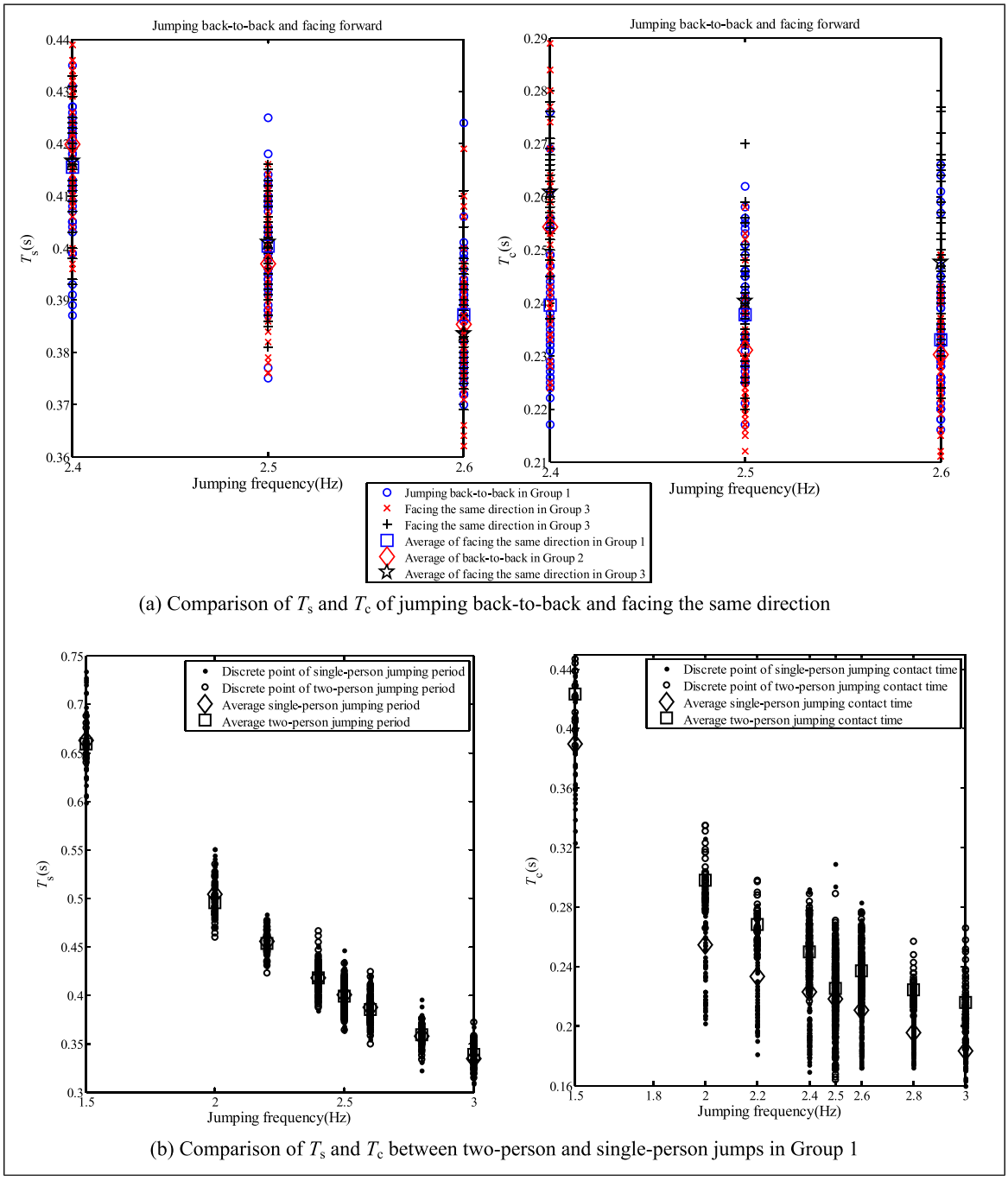

(a) Comparison of T_s and T_c of jumping back-to-back and facing the same direction

(b) Comparison of T_s and T_c between two-person and single-person jumps in Group 1

Figure 19. T_s and T_c distribution of two persons and comparison of single-person jump characteristic parameters.

orientations among spectators include jumping while facing the same direction and jumping back-to-back (the latter typically observed in football grandstands). Accordingly, the experiment measured k_p under these two orientations, as shown in Figure 18(a). The left panel displays k_p values from Group 1, where a total of 1086 data points were recorded. Dots represent jumps while facing the same direction, squares denote back-to-back jumps, and the cross and diamond symbols indicate the corresponding mean values for each mode. The right panel presents k_p values from three subject groups jumping back-to-back, facing the same direction, and face-to-face at 2.5 Hz. It can be seen from Figure 18(a) that the range of k_p values for jumps performed while facing the same direction is wider than for the other modes. However, comparison of the average values reveals no consistent trend, suggesting that k_p is not significantly affected by the jumping mode selected in the experiment.

To further examine the coupling superposition effect of the load during two-person jumping, the k_p values from two-person and single-person jumps were compared, as shown in Figure 18(b). This figure presents a comparison between the superimposed peak ratios obtained by summing the k_p values of two individuals during single-person jumps and the k_p measured during the two-person simultaneous jumps. The figure shows that the k_p distribution range and average value during two persons jumping are significantly lower than the corresponding superimposed values from single-person jumps, with a maximum reduction of 15%. All experimental data followed this trend. Furthermore, results from earlier vertical springboard tests involving two- and three-person simultaneous jumping also showed reductions of 10% and 27.6%, respectively. The two independent experimental setups verify the same phenomenon, reinforcing the conclusion that the coupled impact load generated by multi-person jumping is significantly lower than the superimposed value of individual impact loads. This finding provides valuable insight for the optimal load design of large-scale temporary structures.

In addition to the characteristic parameter k_p, analyzing the impact of IaSV and IeSV on T_s and T_c (corresponding to two-person simultaneous jumping) is also of great significance for the intelligent design of large-scale temporary structures. This paper summarizes and analyzes T_s and T_c values obtained from 2172 two-person simultaneous jumps. The dots in Figure 19(a) represent T_s and T_c values for back-to-back jumping in Group 1, the red crosses represent T_s and T_c values for same direction jumping in Group 1, and the black crosses represent T_s and T_c values corresponding to same direction jumping in Group 3. As seen in the left panel of Figure 19(a), the distribution range of T_s is similar across different jump modes and groups, indicating that jump orientation and group variation have minimal influence on T_s. The average T_s is very close to the theoretical value. A similar trend is observed for T_c in the right panel of Figure 19(a), where the differences in average T_c between groups remain within hundredths of a second. Figure 19(b) compares the T_s and T_c values from single-person and two-person jumping in Group 1. In the left figure, the T_s distributions are nearly identical, with consistent average values and trends. In the right figure, while the distribution range of T_c is broader for single-person jumps, the average value of T_c for two-person jumps is greater. Although the general trend remains the same, the average T_c for two-person jumping is 12.6% higher than that of single-person jumping, indicating that multi-person jumping increases the contact time of the load acting on the structure. Although this conclusion is based on a relatively limited dataset from two-person experiments, it provides valuable insight into the jumping load characteristics of larger spectator crowds. Future work will further investigate the relationship between contact time T_c during load impact in multi-person crowd jumping and the corresponding T_c values observed in single-person jumps.

Through the above analysis of the characteristic parameters from the two-person simultaneous jump tests, it is observed that, compared with single-person jumping, the total load is reduced, the jumping period changes minimally, and the contact

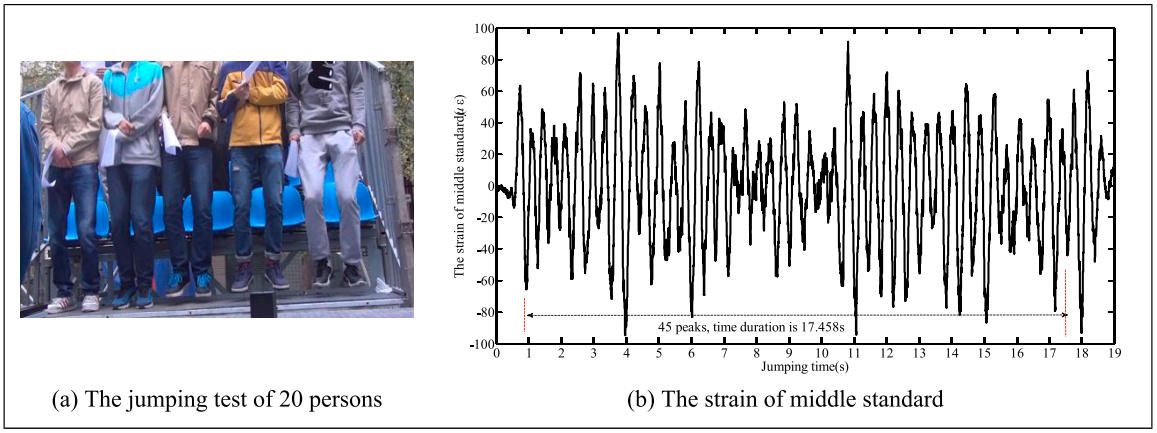

(a) The jumping test of 20 persons (b) The strain of middle standard

Figure 20. Experiment of 20 persons jumped at temporary grandstand.

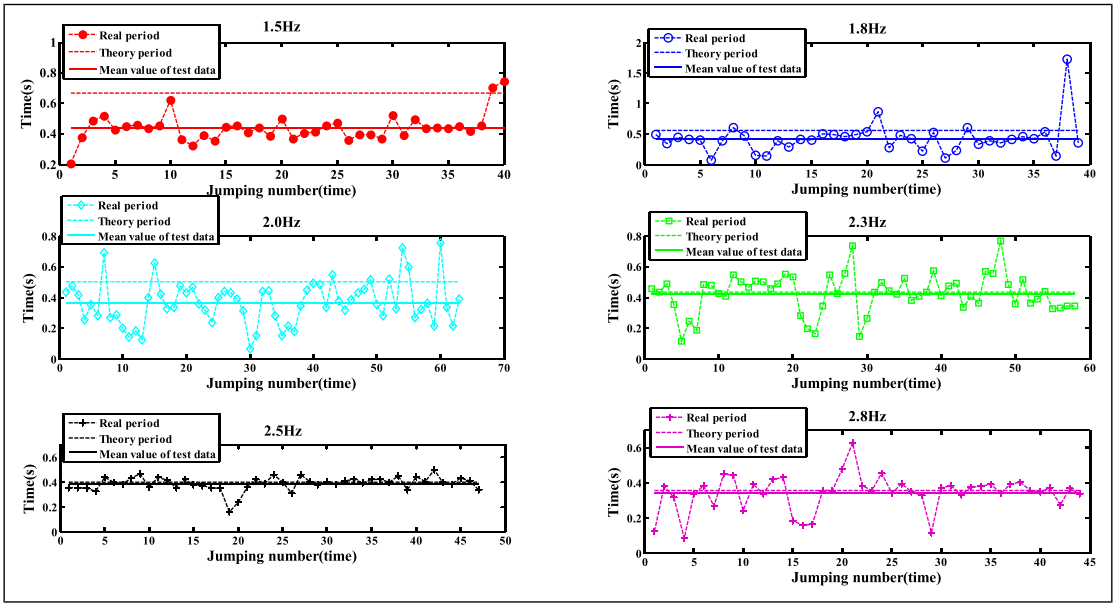

Figure 21. Analysis of crowd jumping periods for 1.5 Hz, 1.8 Hz, 2.0 Hz, 2.3 Hz, 2.5 Hz, 2.8 Hz.

time increases. In existing studies on crowd load analysis, Ji[11] proposed a reduction coefficient method with a value of 0.67, and Comer, based on a 15-person jumping test,[38] concluded that the standard deviation of period variation in multi-person jumping is lower than that in single-person jumping.

Additionally, a test was conducted on a temporary grandstand occupied by 20 participants, who jumped in a standing position at inspired frequencies of 1.5 Hz, 1.8 Hz, 2.0 Hz, 2.3 Hz, 2.5 Hz, and 2.8 Hz. All 20 participants were male, with body masses ranging from 54 to 88 kg, heights between 1.62 m and 1.84 m, and ages ranging from 21 to 26 years old. The tests were preceded by a rigorous risk assessment and were approved by the university's research ethics committee. Two certified first aid officers were present in the laboratory throughout all test sessions. Figure 20(a) shows the crowd jumping on the temporary grandstand. In the front row, not all individuals were airborne simultaneously (three individuals in the air, two in contact with the structure), illustrating the non-synchronous nature of crowd jumping. As a result, the dynamic response curve of the structure (Figure 20(b)) differs significantly from that of a single-person jumping load.

The crowd jumping period is further analyzed in Figure 21. It is shown that the actual crowd jumping period at each instance varies during the active jumping phase guided by a metronome. However, jumping synchrony improves as the jumping frequency increases, particularly at 2.3 Hz, 2.5 Hz, and 2.8 Hz. Table 2 presents the standard deviation and mean values of the crowd's jumping period and frequency, which further confirm this trend.

In this paper, a large amount of single-person jump data was analyzed, and a single-person vertical jumping load model was developed using equations (4) and (5). For two- and three-person jumping tests, it was found that the peak load values decrease, while the contact time increases. In practical scenarios, however, many individuals may be jumping on a structure simultaneously, and each jumping load behaves as a typical random load. Therefore, based on a preliminary statistical estimation approach, it is recommended to use the program provided in Appendix I to simulate multi-person jumping loads.

Table 2. The standard deviation and mean values of crowd jumping period and frequency.

Active frequency (Hz)	The average value of real jumping period time(s)	Standard deviation of period time	The average value of real jumping frequency (Hz)
1.5	0.435	0.10	2.30
1.8	0.429	0.26	2.33
2.0	0.367	0.14	2.72
2.3	0.425	0.13	2.35
2.5	0.387	0.06	2.58
2.8	0.347	0.10	2.88

Spectator jumping horizontal load

When a large number of spectators jump synchronously, the resulting horizontal load can induce significant lateral displacement of the temporary grandstand and may even pose a risk of lateral collapse. Due to the complex relationship between the horizontal load on temporary structures and human motion, no quantitative calculation model has yet been established. Existing studies provide only qualitative estimates, often based on analogical reasoning, and successively calculate the horizontal load. In general, the horizontal load is assumed to be 7%–10%[39] or 20%[40] of the vertical load. The lateral horizontal load of a temporary structure is typically considered as a component of the front-to-back horizontal load. Jumping data from this experiment also clearly reveals the subcomponents of the horizontal load. The three-directional load distribution is shown in Figure 22, representing the horizontal and vertical load components recorded during jumping by Subject No. 5.

The horizontal load curve measured during the single-person jump test is shown in Figure 23(a) (a segment of the curve shown in Figure 22). This figure illustrates that the horizontal load exhibits very weak regularity. Although the overall curve appears pseudo-periodic, the horizontal load lacks clear periodic characteristics, as it primarily reflects the alternating

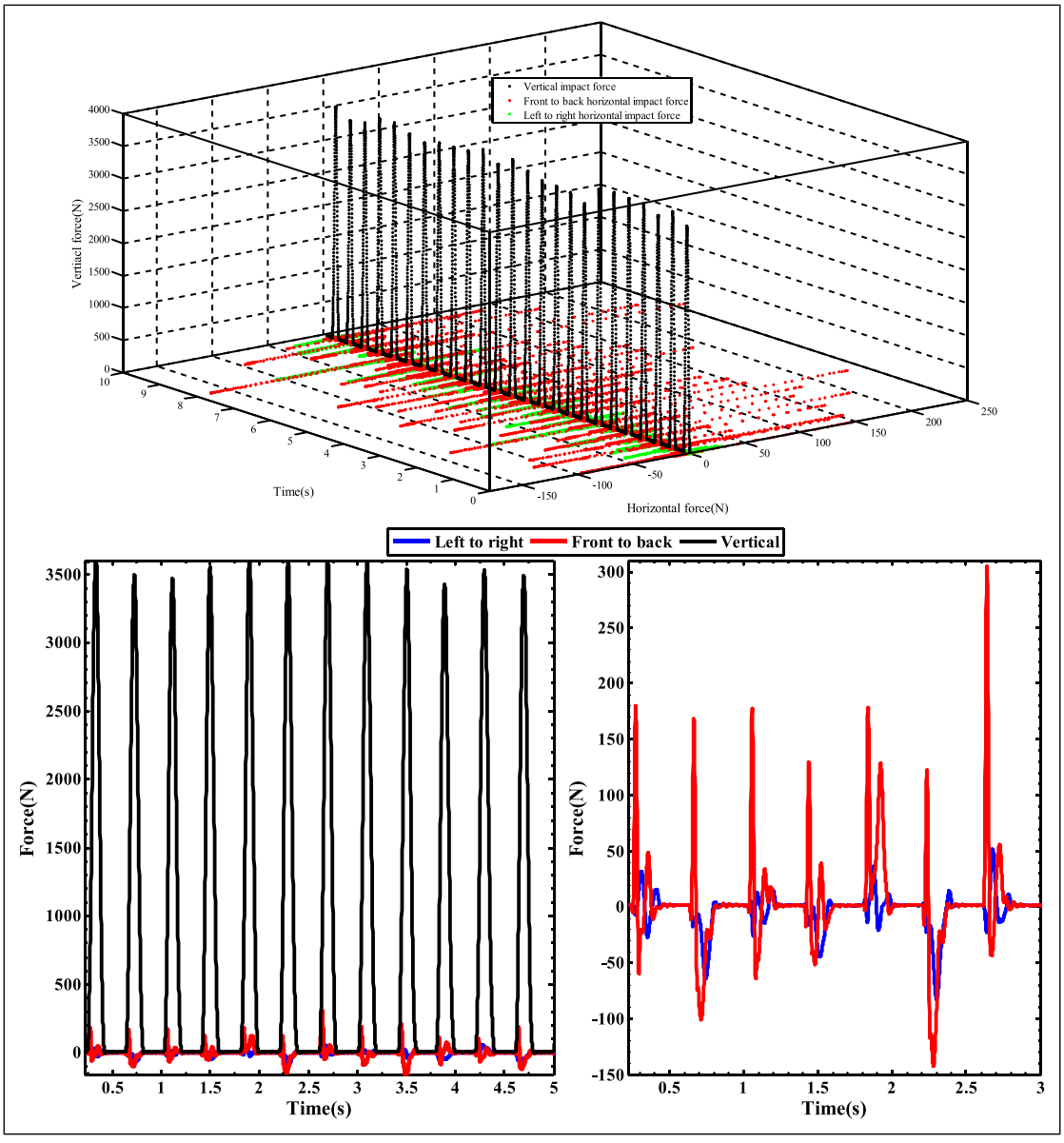

Figure 22. Distribution of three directions of jumping load at 2.5 Hz.

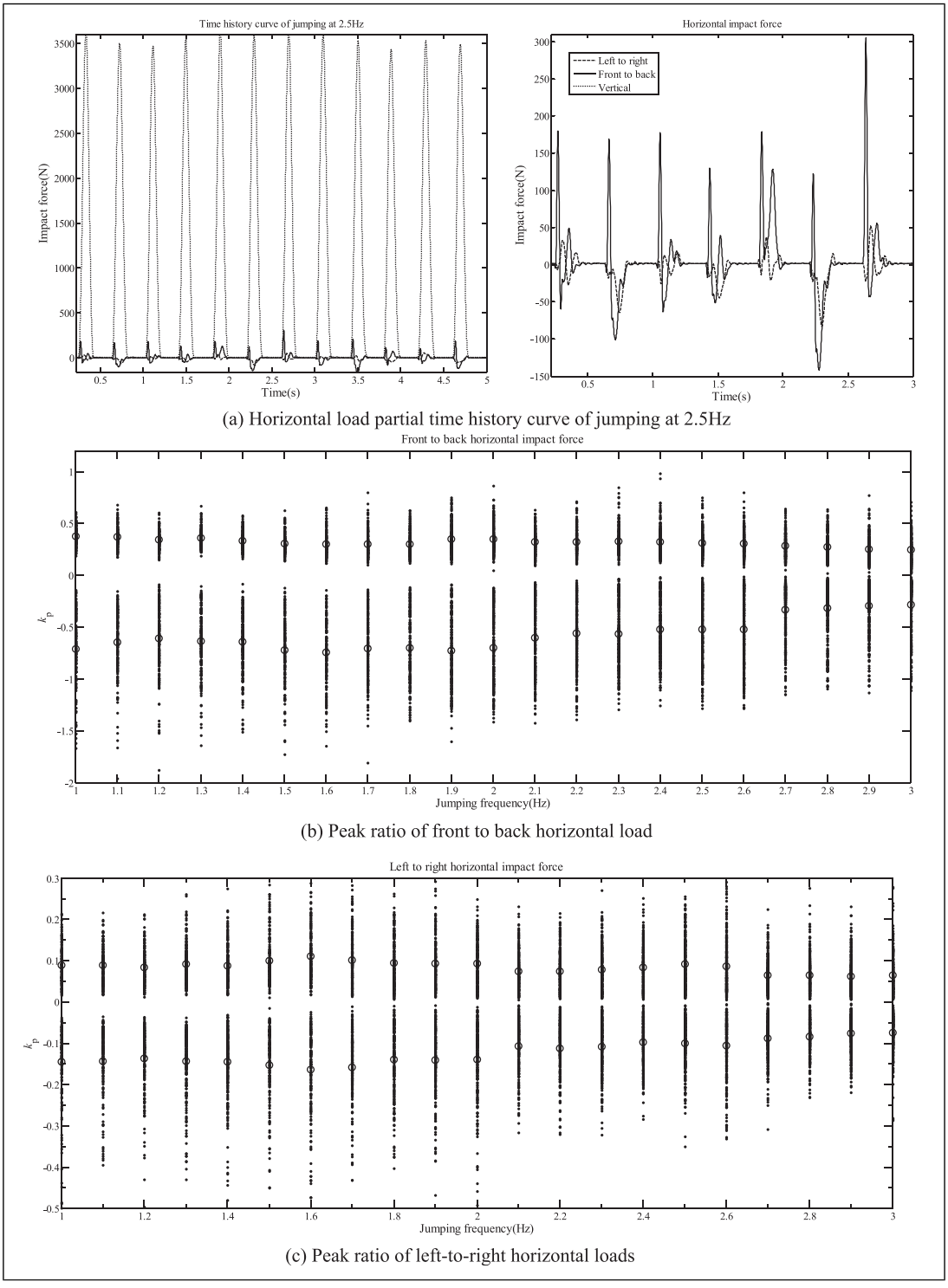

Figure 23. Horizontal load caused by jumping.

directions of the load in the horizontal plane. The left-to-right horizontal load is smaller than the front-to-back horizontal load, and the curves in the two directions do not overlap, indicating that left-to-right loads are independent of front-to-back loads. Statistical analysis of the peak ratio of the horizontal loads in the front-to-back direction (Figure 23(b)) and the left-to-right direction (Figure 23(c)) reveals that the peak ratios decrease with increasing frequency. In Figure 23(b), (a) positive peak ratio represents the load toward the front of the body during take-off, while a negative peak ratio corresponds to the

load toward the back during landing and impact. These opposing signs arise because it is difficult for subjects to maintain a perfectly vertical take-off and landing. Statistical data show that the average negative peak ratio is greater than the positive peak ratio, as the impact force during landing exceeds the reaction force during take-off. The average values of the positive and negative peak ratios are approximately 0.32 and 0.57, respectively, with a total average of 0.45. Similarly, the left-to-right horizontal load peak ratios in Figure 23(c) are lower than those in the front-to-back horizontal loads, as forward/backward inclination is the dominant movement during jumping. The positive and negative average values are 0.08 and 0.12, respectively, with a total average of 0.10.

In order to simplify the calculation, the horizontal jumping load is modeled as a sine curve, with the amplitude defined as the mean peak ratio obtained from Figure 23. T_{si} and T_{ci} are taken from equations (4) and (5), respectively, and obtained from equation (6). Thus, the fitting calculation model of horizontal load is expressed as equation (7):

$$\begin{cases} F_{\text{front to back } i} = G \cdot g \cdot 0.45 \cdot \sin\left(\dfrac{2\pi}{T_{ci}} t\right) t \in [0, T_{ci}] \\ F_{\text{front to back } i} = 0 \, t \in [T_{ci}, T_{si}] \end{cases} \Rightarrow F_{\text{front to back}} = \sum_{i=1}^{N} F_{\text{front to back } i} \tag{7a}$$

$$\begin{cases} F_{left\ to\ right\ i} = G \cdot g \cdot 0.1 \cdot sin\left(\dfrac{2\pi}{T_{ci}} t\right) \ \ t \in [0, T_{ci}] \\ F_{left\ to\ right\ i} = 0 \ \ t \in [T_{ci}, T_{si}] \end{cases} \Rightarrow F_{left\ to\ right} = \sum_{i=1}^{N} F_{left\ to\ right\ i} \tag{7b}$$

Conclusion and discussion

This study proposes a reliable simulation approach for modeling jumping-induced loads on temporary grandstand structures based on force plate experiments. Key findings include the following:

(1) The peak load ratio, jumping period, and contact time are fundamental to quantifying jumping loads. These parameters, along with their residual variations, follow normal distributions and can be modeled probabilistically.
(2) A Haver-based Gaussian multi-peak model effectively replicates the complex, non-periodic shapes of measured jumping loads while reducing computational burden, making it suitable for real-time structural analysis.
(3) Two-person jumping produces a combined load approximately 85% of the sum of individual loads, indicating a significant coupling effect without a linear additive relationship.
(4) Horizontal jumping loads are non-negligible: the front-to-back component averages 45% of body weight, while the left-to-right component averages 10%, highlighting the need to account for multi-directional forces in grandstand design.

Currently, this model requires a relatively large number of parameters for computation. And, further studies on this jumping load model are still required, such as individual jumping forces in this study were tested by a rigid surface, the mechanical mechanism of load coupling effects in scenarios with multiple jumpers at real structures has not yet been clearly defined, postures such as “face-to-face” and the rationality of scenarios for different postures are not mentioned, such postures maybe produce different load coupling effects due to mutual interference. Moreover, regression-based ML model[41] and unsupervised learning[42] are also used to simulate force curve. So, the authors should train a regression-based ML model (e.g., gradient boosting or shallow neural network) and use unsupervised learning (e.g., k-means or DBSCAN) to predict the jumping load curve parameters and identify behavioral patterns among jumpers in forthcoming research investigations. This would enrich the simulation framework by allowing for more realistic, behaviorally diverse crowd load generation.

ORCID iD

Suhui Yu https://orcid.org/0000-0001-6338-226X

Ethical considerations

The authors confirm that all methods were conducted in accordance with institutional laboratory guidelines and regulations. The authors confirm that all experimental protocols were approved by the Key Laboratory of Structural Dynamic Behavior and Control of the Ministry of Education (Harbin Institute of Technology), School of Civil Engineering, Harbin Institute of Technology, Harbin, and the Academy of Combat Support, Rocket Force University of Engineering.

Consent to participate

All participants provided informed consent for the use of photographs in the paper. The research was conducted in compliance with ethical standards and the Declaration of Helsinki.

Funding

The authors disclosed receipt of the following financial support for the research, authorship, and/or publication of this article: For this paper, we are grateful for the support of Project 2014BAK14B05 of the Ministry of Science and Technology. Also, it is supported by Engineering research GCKY-2022002.

Declaration of conflicting interests

The authors declared no potential conflicts of interest with respect to the research, authorship, and/or publication of this article.

Supplemental Material

Supplemental material for this article is available online.

References

1. Meijers W and Hermens M, Measurements and review of grandstand loads.EVACES 2025. Lecture Notes in Civil Engineering, vol 675. Springer, Cham. https://doi.org/10.1007/978-3-031-96106-9_9
2. Xu T, Meijers W, Meijers SJH, et al. Non-linear dynamic analysis of collapsed grandstand. *J Phys: Conf Ser* 2024; 2647: 162003.
3. Xu Man, Gao Shan, Zhang Sumei and Li Honghao. Experimental study on bolted CFST-column joints with different configurations in accommodating column-loss. *Journal of Constructional Steel Research*. 2018; 151: 122–131. doi:10.1016/j.jcsr.2018.09.021.
4. de Brito VL and Pimentel R. Cases of collapse of demountable grandstands. *J Perform Constr Facil* 2009; 23: 151–159.
5. BS 6399-1:1996. *Loading for buildings*. British Standards Institution, 1996.
6. BS EN 1991-1:2002. *Eurocode 1 actions on structures. General actions. Densities, self-weight, imposed loads for buildings*. British Standards Institution, 2002.
7. BRE Digest 426. *The response of structure to dynamic crowd loads*. Building Research Establishment, 1997.
8. BRE Digest 426. *The response of structure to dynamic crowd loads*. Building Research Establishment, 2004.
9. NRCC47666. *National building code of Canada*. National Research Council of Canada, 2005.
10. Bachmann H and Ammann W. *Vibrations in structures induced by man and machines*. IABSE–AIPC–IVBH, 1987.
11. Ji T and Ellis BR. Evaluation of dynamic crowd effects for dance loads. *Proceedings of IABSE international colloquium on structural serviceability of buildings*. Goteborg, 1993, pp. 165–172.
12. Wang Jing-xuan, Shen Ya-jun, Gao Shan and Wang Wen-da. Anti-collapse performance of concrete-filled steel tubular composite frame with assembled tensile steel brace under middle column removal. *Engineering Structures*. 2022; 266: 114635. doi:10.1016/j.engstruct.2022.114635.
13. Brownjohn JMW, Pavic A and Omenzetter P. A spectral density approach for modelling continuous vertical forces on pedestrian structures due to walking. *Can J Civ Eng* 2004; 31: 65–77.
14. Parkhouse JG and Ewins DJ. Crowd induced rhythmic loading. *Proceedings of the Institution of Civil Engineers, Structures and Buildings* 2006; 159(SB5): 247–259.
15. Kasperski M and Agu E. *Prediction of crowd-induced vibrations via simulation*. In: 23rd international modal analysis conference, Orlando, FL, USA: IMAC XXIII, 2005.
16. Sim JH. *Human-structure interaction in cantilever grandstands*. University of Oxford, 2006. PhD thesis.
17. Gao Shan. Life cycle sustainability assessment of concrete-filled steel tubular frames in earthquake regions. *Engineering Structures*. 2025; 328: 119761. doi:10.1016/j.engstruct.2025.119761.
18. Sim JH, Blakeborough A, Williams M, et al. Statistical model of crowd jumping loads. *J Struct Eng* 2008; 134: 1852–1861.
19. Racic V and Pavic A. Mathematical model to generate asymmetric pulses due to human jumping. *J Eng Mech* 2009; 135: 1206–1211.
20. Racic V and Pavic A. Mathematical model to generate near-periodic human jumping force signals. *Mech Syst Signal Process* 2010; 24: 138–152.
21. Racic V and Pavic A. Stochastic approach to modelling of near-periodic jumping loads. *Mech Syst Signal Process* 2010; 24: 3037–3059.
22. Wang L. *Experimental and model study on dynamic properties of human jumping load*. Shanghai Tongji University, 2012.
23. Zhao Y. *Experimental modeling of humans jumping load and its applications*. Shanghai Tongji University, 2013.
24. Chen J, Wang H and Wang L. Experimental investigation on single person's jumping load model. *Earthq Eng Eng Vib* 2015; 14(4): 703–714.

25. Chen J, Wang L, Chen B, et al. Experimental study on dynamic characteristics and load model of jump loads. *J Vib Eng* 2014; 27(1): 16–24.
26. Gao Shan, Xu Youchun, Zhang Sumei and Derlataka Anna. Performance of square concrete-filled steel tubular columns under repeated lateral impact. *Engineering Structures*. 2023; 280: 115719. doi:10.1016/j.engstruct.2023.115719.
27. Tan H, Zhao Y and Chen J. Experimental investigation on coherency factor of crowd jumping load and its application. *Eng Mech* 2016; 33(2): 145–151.
28. Chen J and Xiong J. Power spectral density model for human jumping load. *China Civ Eng J* 2018; 51(9): 56–65.
29. Vijayan A, Abraham NM and Anitha Kumari SD. Analysis of structures subjected to crowd loads. *Procedia Struct Integr* 2019; 14: 696–704.
30. Yuan J, He L, Fan F, et al. Dynamic modeling and vibration analysis of temporary grandstand due to crowd-jumping loads. In: The proceedings of the 9th international conference on structural dynamics, Portugal, Porto, 30 June–2 July 2014, 2014.
31. Yuan J, He L, Fan F, et al. The dynamic parameters of passive human at temporary demountable grandstands during exposure to lateral vibration. *J Civ Eng Manag* 2018; 24(4): 265–283.
32. He L, Yuan J, Fan F, et al. Dynamic forces of swaying human and responses of temporary demountable grandstand based on experiment and simulation. *Shock Vib* 2018; 1: 22.
33. Lasowicz N, Falborski T and Jankowski R. Analysis of temporary steel grandstand with different bracing systems exposed to crowd load. *J meas eng* 2018; 6(4): 256–262.
34. Ginty D, Dervent JM and Ji T. The frequency ranges of dance-type loads. *Struct Eng* 2001; 79(6): 27–31.
35. Littler JD. Frequencies of synchronized human loading from jumping and stamping. *Struct Eng*. 2001; 81(22): 27–35.
36. DGJ08-114-2005. *Technical regulations for the application of temporary buildings (structures) (trial)*. Shanghai Engineering Construction Code, 2005.
37. O'Haver T. *Peakfit.m, version 4.21, department of chemistry and biochemistry.* The University of Maryland at College Park, 2013.
38. Comer AJ, Williams MS and Blakeborough A. Experimental determination of crowd load and coherency when jumping on a rigid raked grandstand, Event25th Conference and Exposition on Structural Dynamics 2007, IMAC-XXV - Orlando, FL, United States.
39. Ellis B, Ji T and Littler JD. The response of grandstands to dynamic crowd loads, structure and buildings. In: *Proceeding of the institution of civil engineers*. ICE, 2000, vol 140, pp. 307–314.
40. Pavic A. Verification of the existence of human-induced horizontal force due to vertical jumping. *IMAC* 2002; 1: 120–126.
41. Duan S, Xiong J and Qian H. Generative adversarial networks-based stochastic approach to the modeling of individual jumping loads. *Int J Struct Stabil Dynam* 2021; 21(04): 2150047.
42. Zheng L, Zhang Q and Fan F. A stochastic approach for generating individual jumping loads considering different jumping force patterns. *J Build Eng* 2022; 62(15 December): 105378.